



# Quiescent cells maintain active degradation-mediated protein quality control requiring proteasome, autophagy, and nucleus-vacuole junctions

Received for publication, July 1, 2024, and in revised form, October 16, 2024. Published, Papers in Press, November 29, 2024.

<https://doi.org/10.1016/j.jbc.2024.108045>

Dina Franić<sup>1,‡</sup>, Mihaela Pravica<sup>1,‡</sup>, Klara Zubčić<sup>1</sup> , Shawna Miles<sup>2</sup>, Antonio Bedalov<sup>2,3</sup>, and Mirta Boban<sup>1,\*</sup> 

From the <sup>1</sup>University of Zagreb School of Medicine, Croatian Institute for Brain Research, Zagreb, Croatia; <sup>2</sup>Translational Science and Therapeutics Division and Human Biology Division, Fred Hutchinson Cancer Center, Seattle, Washington, USA; <sup>3</sup>Department of Medicine and Department of Biochemistry, University of Washington, Seattle, Washington, USA

Reviewed by members of the JBC Editorial Board. Edited by George DeMartino

Many cells spend a major part of their life in quiescence, a reversible state characterized by a distinct cellular organization and metabolism. In glucose-depleted quiescent yeast cells, there is a metabolic shift from glycolysis to mitochondrial respiration, and a large fraction of proteasomes are reorganized into cytoplasmic granules containing disassembled particles. Given these changes, the operation of protein quality control (PQC) in quiescent cells, in particular the reliance on degradation-mediated PQC and the specific pathways involved, remains unclear. By examining model misfolded proteins expressed in glucose-depleted quiescent yeast cells, we found that misfolded proteins are targeted for selective degradation requiring functional 26S proteasomes. This indicates that a significant pool of proteasomes remains active in degrading quality control substrates. Misfolded proteins were degraded in a manner dependent on the E3 ubiquitin ligases Ubr1 and San1, with Ubr1 playing a dominant role. In contrast to exponentially growing cells, the efficient clearance of certain misfolded proteins additionally required intact nucleus-vacuole junctions (NVJ) and Cue5-independent selective autophagy. Our findings suggest that proteasome activity, autophagy, and NVJ-dependent degradation operate in parallel. Together, the data demonstrate that quiescent cells maintain active PQC that relies primarily on selective protein degradation. The necessity of multiple degradation pathways for the removal of misfolded proteins during quiescence underscores the importance of misfolded protein clearance in this cellular state.

Misfolded proteins can interfere with essential cellular processes and give rise to disease, such as Alzheimer's, Parkinson's, and others (1–5). The protein quality control (PQC) system, a complex network of evolutionarily conserved pathways, prevents the accumulation of misfolded proteins by mediating protein refolding, selective degradation, and spatial sequestration to inclusions (1, 4, 6–8).

Terminally misfolded proteins are posttranslationally modified by polyubiquitin and subsequently targeted for degradation to the proteasomes. Protein ubiquitination is catalyzed by a series of enzymes, including ubiquitin-conjugating enzymes (E2) and ubiquitin-protein ligases (E3) (9). The primary determinants of ubiquitination specificity are the E3 ubiquitin ligases, in many cases in cooperation with molecular chaperones (10). In yeast, the principal E3 ubiquitin ligases that target cytoplasmic misfolded proteins for degradation are Ubr1, a protein found in the cytoplasm and nucleus, a nuclear E3 ligase San1, and Doa10, the integral membrane E3 ligase of the endoplasmic reticulum and the inner nuclear membrane (11–18). The selectivity of proteasome degradation is achieved by the ubiquitin-binding receptors present in the 19S regulatory particle, while the substrates are cleaved by the proteolytic enzymes present within the 20S core particle (19). The 19S particles also contain ATPases that facilitate substrate unfolding and entry into the 20S core particle. In addition, 19S particles contain deubiquitinating enzymes that remove ubiquitin from the substrate prior to its entry into the 20S core particle, thereby facilitating substrate degradation (20).

Under the conditions of misfolded protein overload, such as in the case of proteasome inhibition or non-functional protein ubiquitination, cells can sequester misfolded proteins into subcellular deposition sites called INQ (intranuclear quality control compartment), JUNQ (juxtannuclear quality control compartment), and CytoQ (cytoplasmic quality control compartment) (21–26). These inclusions are dynamic (21, 22), and from there, misfolded proteins can be disaggregated and directed to refolding or degradation (27). In contrast, cytoplasmic insoluble protein deposits (IPOD) are cytoplasmic inclusions that terminally sequester insoluble misfolded proteins with amyloid-like properties (8, 21).

Due to the structural restraints of the translocation channel, only individual proteins that have been unfolded by the ATPases in the 19S regulatory particle can be degraded by the proteasome (20), while larger assemblies or protein aggregates can be degraded by autophagy (28). In the process of autophagy, cargo material is enclosed by autophagosomes, double-membrane vesicles decorated with the ubiquitin-like protein

<sup>‡</sup> These authors contributed equally to this work.

\* For correspondence: Mirta Boban, [mirta.boban@hiim.hr](mailto:mirta.boban@hiim.hr).

## Protein quality control in quiescence

Atg8, and delivered to the lysosomal compartment, or vacuole in yeast (29). The formation of autophagosomes is mediated by a set of conserved proteins, collectively termed the core machinery. In non-selective or bulk autophagy, autophagosome biogenesis is triggered by nutrient starvation, including glucose depletion (29). In selective autophagy, autophagosome biogenesis can be triggered even in the absence of starvation, by cargo receptors or autophagy receptors, which simultaneously bind cargo marked by a specific modification, such as ubiquitin, and Atg8 present on the autophagosomal membrane (30).

In nature, many cells spend a considerable amount of their lifetime in a reversible non-dividing state known as quiescence, which is characterized by a distinct cellular organization and metabolism (31–34). When incubated in a rich glucose-based medium, yeast *Saccharomyces cerevisiae* grows exponentially until glucose is exhausted. At that point, the culture undergoes a diauxic shift, cells switch to utilizing a non-fermentable carbon source, such as ethanol, and enter into quiescence (31, 35). Finally, upon exhaustion of the carbon source, cells cease dividing entirely, and the culture enters the stationary phase.

In contrast to dividing yeast cells, in which the majority of the proteasomes accumulate in the nucleus (36), in quiescent cells, proteasomes relocate to the nuclear periphery and to cytoplasmic condensates called proteasome storage granules (37), which are thought to contain inactive proteasomes disassembled into core and regulatory particles (38, 39). How quiescent cells manage protein quality control substrates has remained unclear. Previous reports using stationary phase cultures have indicated the accumulation of misfolded proteins within inclusions (40) and a decline in the degradation of proteasomal substrates (39, 41). However, due to the barely detectable protein expression levels observed (39), the interpretation of the results was challenging.

In this study, we investigated whether quiescent cells retain degradation-mediated protein quality control, by expressing model misfolded proteins in quiescent cells of yeast *S. cerevisiae*. We report that quiescent cells target misfolded proteins for selective degradation by the proteasome, suggesting that a significant pool of the 26S proteasomes remain actively engaged in the degradation of quality control substrates during cell quiescence. Moreover, the efficient elimination of certain misfolded proteins was additionally dependent on the intact nucleus-vacuole junctions (NVJ) and core autophagy machinery. The requirement for the functional autophagy was substrate-specific, indicating selectivity, and was independent of the known yeast ubiquitin-binding cargo receptor Cue5. Together, our results indicate that degradation-mediated PQC is sustained during cell quiescence and chronological aging.

## Results

### Glucose-depleted quiescent yeast cells retain degradation-mediated protein quality control

To investigate whether quiescent cells retain degradation-mediated protein quality control, we analyzed cytoplasmic

misfolded proteins tGnd1 (truncated Gnd1) and stGnd1 (small truncated Gnd1), C-terminally truncated versions of yeast 6-phosphogluconate dehydrogenase enzyme Gnd1, that arise due to a premature stop codon in *GND1* gene (11). We expressed HA-epitope tagged tGnd1 and stGnd1 in quiescent yeast cells and examined protein stability by cycloheximide chase experiment (Fig. 1). Genes encoding s/tGnd1-HA were placed under the control of the constitutive *PIR3* promoter, which becomes active upon cell entry into quiescence (Fig. S1). Additionally, we analyzed exponentially growing cells that expressed s/tGnd1-HA from the constitutive *TEF1*-gene promoter. Cell cultures grown under identical conditions were tested for cell density, glucose, and ethanol concentration at different time points, showing that by the time point of 24 h after culture inoculation, cells had consumed all glucose (Fig. 1A). Ethanol was consumed by day five, which coincided with the complete cessation of cell growth, indicating cell culture entry into the stationary phase. In contrast to the wild-type protein Gnd1, which was stable, model misfolded proteins tGnd1-HA and stGnd1-HA expressed in cells from two-day-old culture were unstable, indicating selective degradation of misfolded proteins, similarly as in exponentially growing cells (Fig. 1B). Misfolded proteins s/tGnd1 were also selectively degraded in a yeast strain of a different genetic background, W303 (Fig. 1C). Together, the data indicate that glucose-depleted quiescent yeast cells maintain degradation-mediated protein quality control.

Cultures entering quiescence are heterogeneous and two fractions can be separated based on different cell densities (42). To examine whether misfolded proteins are targeted for degradation in cells from both density fractions, the cells were separated by centrifugation in the density gradient (Fig. 1D). The use of a progesterone-inducible Z-promoter enabled s/tGnd1 expression at later stages of cell quiescence. The analysis demonstrated that tGnd1 and stGnd1 undergo degradation in cells from both density fractions (Fig. 1D). Moreover, the stability of tGnd1 and stGnd1 in cells from five-day-old cultures was similar to that observed in cells from two-day-old cultures (Fig. 1E), indicating that the degradation of misfolded proteins persists throughout the later stages of quiescence.

### Protein quality control in quiescent cells involves an active ubiquitin-proteasome system and spatial sequestration of misfolded proteins to inclusions

In exponentially growing cells, tGnd1 and stGnd1 are targeted for degradation by the activity of E3 ligases San1 and Ubr1 (11). To test whether selective degradation of s/tGnd1 in quiescent cells also requires the activity of the same E3 ubiquitin ligases, we examined the stability of tGnd1-HA and stGnd1-HA expressed in single *ubr1Δ* and *san1Δ* mutants, and the double *san1Δ ubr1Δ* mutant (Fig. 2). In exponentially growing cells, stGnd1 was mainly targeted by the E3 ubiquitin ligase Ubr1, while efficient stabilization of tGnd1 required the deletion of both *SAN1* and *UBR1* (Fig. 2, A and B), which is consistent with a previous study (11). In quiescent cells, in

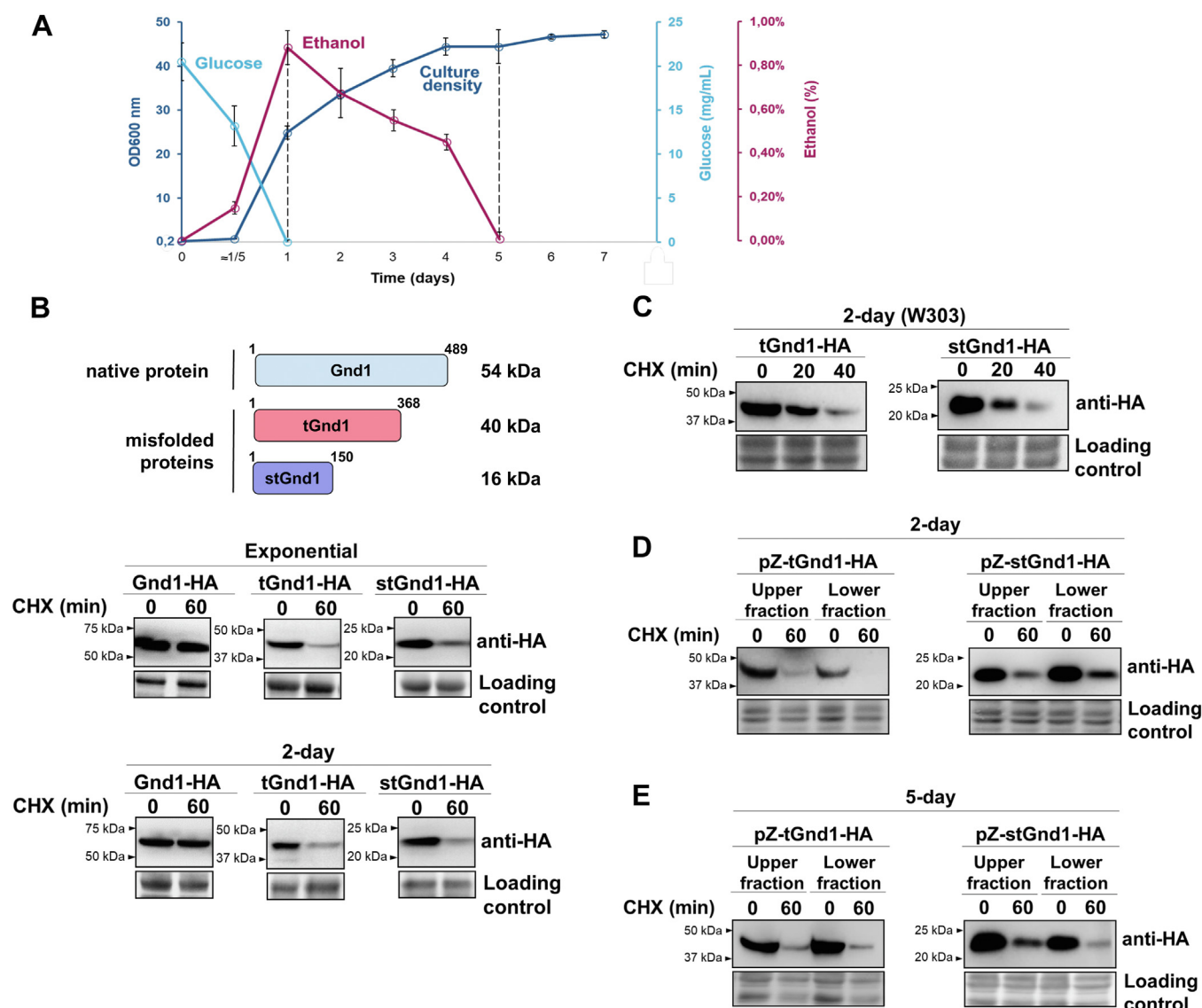


**Figure 1. Quiescent yeast cells target misfolded proteins tGnd1 and stGnd1 for selective degradation.** *A*, growth curve of yeast strain BY4741 in complete liquid medium YPD with 2% glucose. Cells were inoculated at an initial optical density of OD<sub>600</sub> 0.2 and cultured for 7 days without media change. Optical density and concentration of glucose and ethanol were measured at indicated time points. Results are presented as mean value  $\pm$  standard deviation ( $n = 3$ ). *B–E*, protein stability was analyzed by cycloheximide (CHX) chase. Cells were collected at indicated time points after cycloheximide addition and analyzed by Western blot (anti-HA). Total proteins were visualized using stain-free technology (Bio-Rad) and used as a loading control. *B*, cells of the wild type yeast strain BY4741 expressing Gnd1-HA (DFY006), tGnd1-HA (DFY004) or stGnd1-HA (DFY005) from *TEF1*-gene promoter were analyzed in exponentially growing cultures ("exponential"). Cells expressing Gnd1-HA (DFY003), tGnd1-HA (DFY001) or stGnd1-HA (DFY002) from *PIR3*-gene promoter were analyzed in cultures grown for 48 h after inoculation ("2-days"). *C*, cells of the wild type yeast strain W303 expressing tGnd1-HA (MPY166) and stGnd1-HA (MPY167) from the *PIR3*-promoter were grown for 48 h ("2-days") and examined as above. *D* and *E*, tGnd1 and stGnd1 are degraded in two-day- and five-day-old cells from both density fractions. Cells expressing tGnd1-HA (DFY052) or stGnd1-HA (DFY053) under the control of a progesterone-inducible pZ promoter were grown for two (*D*) or five (*E*) days, expression was induced by the addition of 100  $\mu$ M progesterone for 60 min before performing cycloheximide chase. Cells were separated in a density-gradient and upper and lower density fractions were analyzed by Western blot.

which protein expression was regulated by the *PIR3*-promoter or a progesterone-inducible Z promoter, the degradation of tGnd1 was more dependent on Ubr1, than on San1, particularly when tGnd1 was constitutively expressed from the *PIR3*-promoter (Fig. S2A). *SAN1* and *UBR1* mRNA analysis showed that in quiescent cells, the levels of both *SAN1* and *UBR1* were decreased to around 40% of the levels present in exponentially growing cells (Fig. S2), therefore it is unlikely that the predominant dependency of tGnd1 degradation on Ubr1 is due to low levels of San1 in quiescent cells. Instead, our results

suggest that in quiescent cells, tGnd1 becomes less accessible to ubiquitination by San1, especially upon prolonged expression. Degradation of stGnd1 in quiescent cells remained predominantly Ubr1-dependent, as in exponentially growing cells (Fig. 2B).

A previous study has shown that tGnd1 expressed in exponentially growing cells of the *san1 $\Delta$  ubr1 $\Delta$*  mutant forms inclusions (22), while the localization of stGnd1 has not been previously tested. To investigate whether s/tGnd1-HA form inclusions in quiescent cells, proteins were N-terminally

## Protein quality control in quiescence

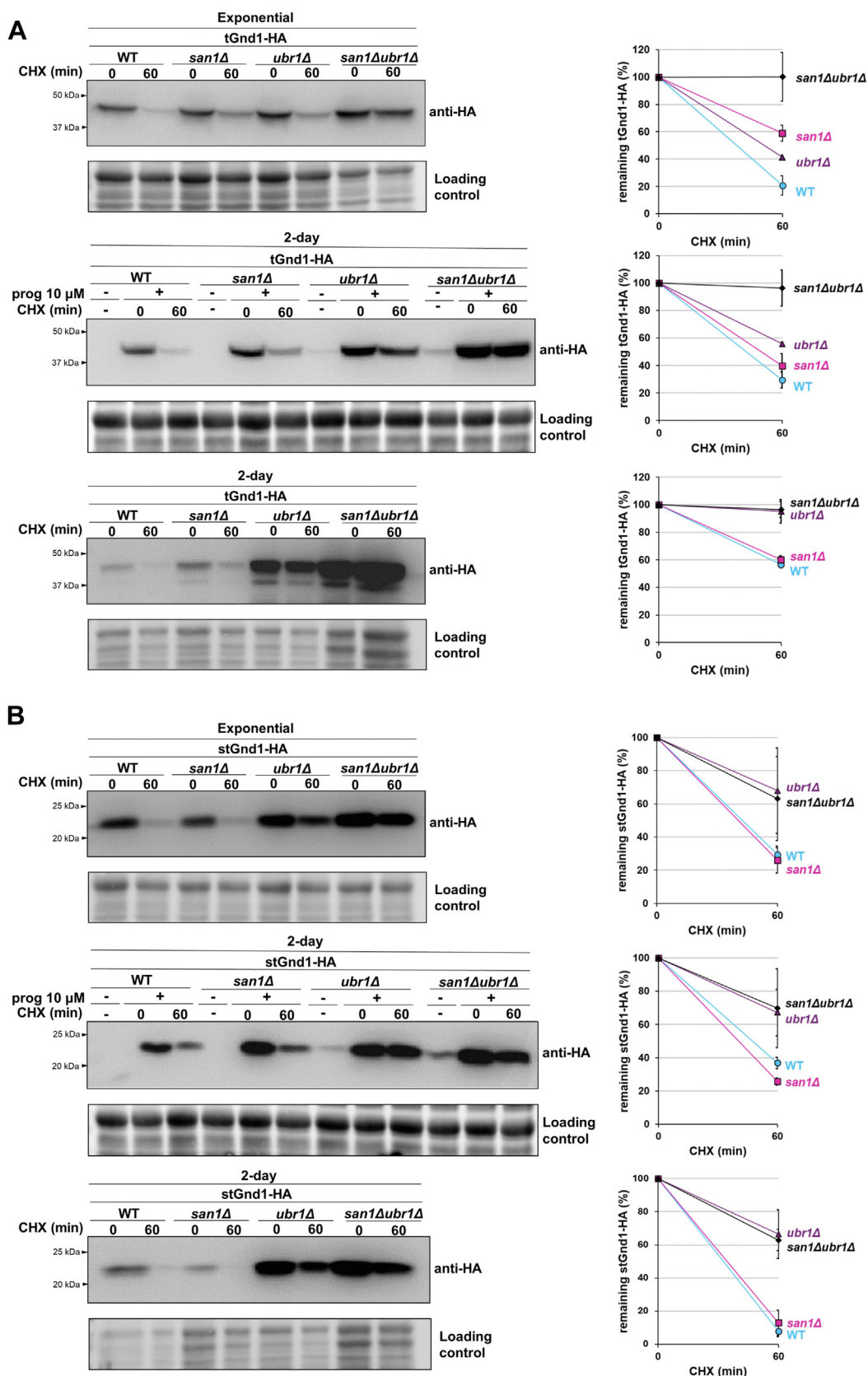


**Figure 2. Degradation of misfolded proteins tGnd1 and stGnd1 in quiescent cells depends predominantly on Ubr1, whereas San1 plays a minor role.** Western blot analysis of the cycloheximide chase (CHX). Cells from exponentially growing cultures (“exponential”) expressing indicated proteins from the constitutive *TEF1*-promoter (A and B, upper panels) and cells from 2-day old cultures expressing indicated proteins from the constitutive *PIR3*-promoter (A and B, lower panels) or progesterone-inducible pZ-promoter (A and B, middle panels) were analyzed as in Figure 1. Graphs represent tGnd1-HA and stGnd1-HA protein levels as a percentage of the protein present at the time point 0 min. Average values and standard deviation are shown (n = 2). A, upper

tagged with the green fluorescent protein ymNeonGreen (NGreen) (43). Analysis of the protein stability by Western blot demonstrated that the degradation of NGreen-tagged constructs was almost entirely dependent on Ubr1 (Fig. 3, A and B), in a manner similar to that previously observed for HA-tagged constructs (Fig. 2, A and B).

The fluorescent signal of NGreen-tGnd1 and NGreen-stGnd1 expressed in the quiescent cells of the wild-type strain was weak. Nevertheless, a small percentage of the cells expressing NGreen-tGnd1, exhibited discrete puncta (Fig. 3A), while NGreen-stGnd1 localized diffusely (Fig. 3B). In the *san1Δ* mutant, the localization of tGnd1 was similar to that observed in the wild-type strain, consistent with the lack of protein stabilization in the single *san1Δ* mutant (Fig. 3A, upper panel). In contrast, in the *ubr1Δ* mutant, tGnd1 formed large inclusions, and their number and the size were further increased in the double *san1Δ ubr1Δ* mutant (Fig. 3A). Furthermore, in addition to a single large inclusion of tGnd1, several smaller puncta were clearly visible in the *san1Δ ubr1Δ* mutant cells. The appearance of the small puncta is consistent with the ongoing protein synthesis of NGreen-tGnd1-HA in our experimental setup and with the previous reports of Q-bodies, small dynamic structures that initially sequester misfolded proteins and eventually coalesce into larger inclusions (23, 24).

In contrast to NGreen-tGnd1, which formed distinct inclusions, NGreen-stGnd1 retained a predominantly diffuse localization, even in the ubiquitination mutants *ubr1Δ* and *san1Δ ubr1Δ*, which exhibit protein stabilization on Western blot (Fig. 3B). In accordance with the dependence of stGnd1 degradation on Ubr1, the double mutation *san1Δ ubr1Δ* did not result in an additive effect. In addition to its predominantly diffuse localization, small granules of stGnd1 could also be detected, however, their low intensity and appearance was clearly different from the large and prominent inclusions of tGnd1. Interestingly, stGnd1 appeared to be slightly enriched in the nuclei of *ubr1Δ* and *san1Δ ubr1Δ* mutants. Nuclear enrichment was not visible in the wild-type, possibly due to low stGnd1 protein levels, therefore it is unclear whether stGnd1 gains access to the nucleus in cells with functional degradation pathways. In summary, tGnd1 localizes to the inclusions, which exhibit a considerable increase in size and frequency in the ubiquitination mutants, whereas stGnd1 localization remains predominantly diffuse even in mutants with impaired protein degradation.

Next, we set out to test whether the degradation of misfolded proteins in quiescent cells involves 26S proteasomes. In contrast to the dividing yeast cells, in which the majority of the proteasomes localize to the nucleus (36), in quiescent cells a large pool of the proteasomes relocates to the nuclear periphery and to the cytoplasmic storage granules, which are thought to contain inactive proteasomes that are disassembled

into core and regulatory particles (38, 39). To investigate whether quiescent cells retain proteasomal degradation of misfolded proteins, we examined the degradation of s/tGnd1 in the proteasomal mutant *rpn11-m1* (44), which expresses non-functional Rpn11, a deubiquitinase that is critical for the functioning of the 26S proteasome (20) (Fig. 4). The *rpn11-m1* mutant is temperature sensitive, therefore the cells were grown at 25 °C and shifted to 37 °C for 30 min prior to the cycloheximide chase. The analysis demonstrated that tGnd1 and stGnd1 were stabilized in the *rpn11-m1* mutant (Fig. 4, A and B), indicating the crucial role of fully assembled and functionally active 26S proteasome in the degradation of misfolded proteins in quiescent cells. Together, the data indicate that the 26S proteasomes remain actively engaged in the degradation of quality control substrates during cell quiescence.

#### Degradation of certain misfolded proteins in quiescent cells requires Cue5-independent autophagy pathway

Cells cultured in a rich glucose-based medium gradually exhaust glucose and switch to using accumulated ethanol as a carbon source (31). Autophagy is induced starting at the ethanol-utilizing phase (45), and can be observed through the accumulation of free GFP in cells expressing GFP-Atg8 (46) (Fig. 5A). To examine whether the degradation of misfolded proteins in quiescent yeast cells requires functional autophagy, we compared the stability of tGnd-HA and stGnd1-HA expressed in wild-type and autophagy-deficient *atg1Δ* and *atg8Δ* mutant strains. The lack of Atg1 and Atg8 did not affect the degradation of stGnd1, indicating that autophagy is not a major pathway for the degradation of stGnd1 in quiescent cells (Fig. 5C). The stability of the cytoplasmic enzyme Pgl1 was also unaffected. In contrast, tGnd1 was stabilized in both *atg1Δ* and *atg8Δ* mutant strains (Fig. 5B), indicating the critical requirement for functional autophagy in the degradation of tGnd1. A similar stabilization of tGnd1 was observed in the *atg1Δ* mutant of another strain background, W303 (Fig. S3).

The data shows that tGnd1, but not stGnd1 or Pgl1, is stabilized in autophagy mutants, suggesting degradation selectivity. In yeast, selective autophagy of aggregation-prone proteins is mediated by the ubiquitin- and Atg8-binding protein Cue5, the only known ubiquitin-binding autophagy receptor in this organism (47, 48). To test the involvement of Cue5, we examined the stability of tGnd1 in a *cue5Δ* deletion mutant, however, there was no effect (Fig. 5D), suggesting a distinct, Cue5-independent, mechanism for autophagy selectivity.

#### The clearance of specific misfolded proteins in quiescent cells critically depends on the intact nucleus-vacuole junctions

A recent study showed that the clearance of deposition sites INQ and JUNQ involves their vacuolar targeting through the nucleus-vacuole junction (NVJ) (24), a site formed by direct

panel, tGnd1-HA in the wild type BY4741 (DFY004), *san1Δ* (DFY039), *ubr1Δ* (DFY043) and *ubr1Δ san1Δ* (DFY057). A, middle panel, tGnd1-HA in wild-type (DFY052), *san1Δ* (DFY118), *ubr1Δ* (DFY119), and *ubr1Δ san1Δ* (DFY120). A, lower panel, tGnd1-HA in wild type (DFY001), *san1Δ* (DFY037), *ubr1Δ* (DFY041) and *ubr1Δsan1Δ* (DFY055). B, upper panel, stGnd1-HA in wild-type strain (DFY005), *san1Δ* (DFY040), *ubr1Δ* (DFY044), and *ubr1Δsan1Δ* (DFY058). B, middle panel, stGnd1-HA in wild-type (DFY053), *san1Δ* (DFY121), *ubr1Δ* (DFY122), and *ubr1Δ san1Δ* (DFY123). B, lower panel, stGnd1-HA in wild-type (DFY002), *san1Δ* (DFY038), *ubr1Δ* (DFY048), and *ubr1Δ san1Δ* (DFY056). Stain-free total protein (Bio-Rad) was used as a loading control.

## Protein quality control in quiescence

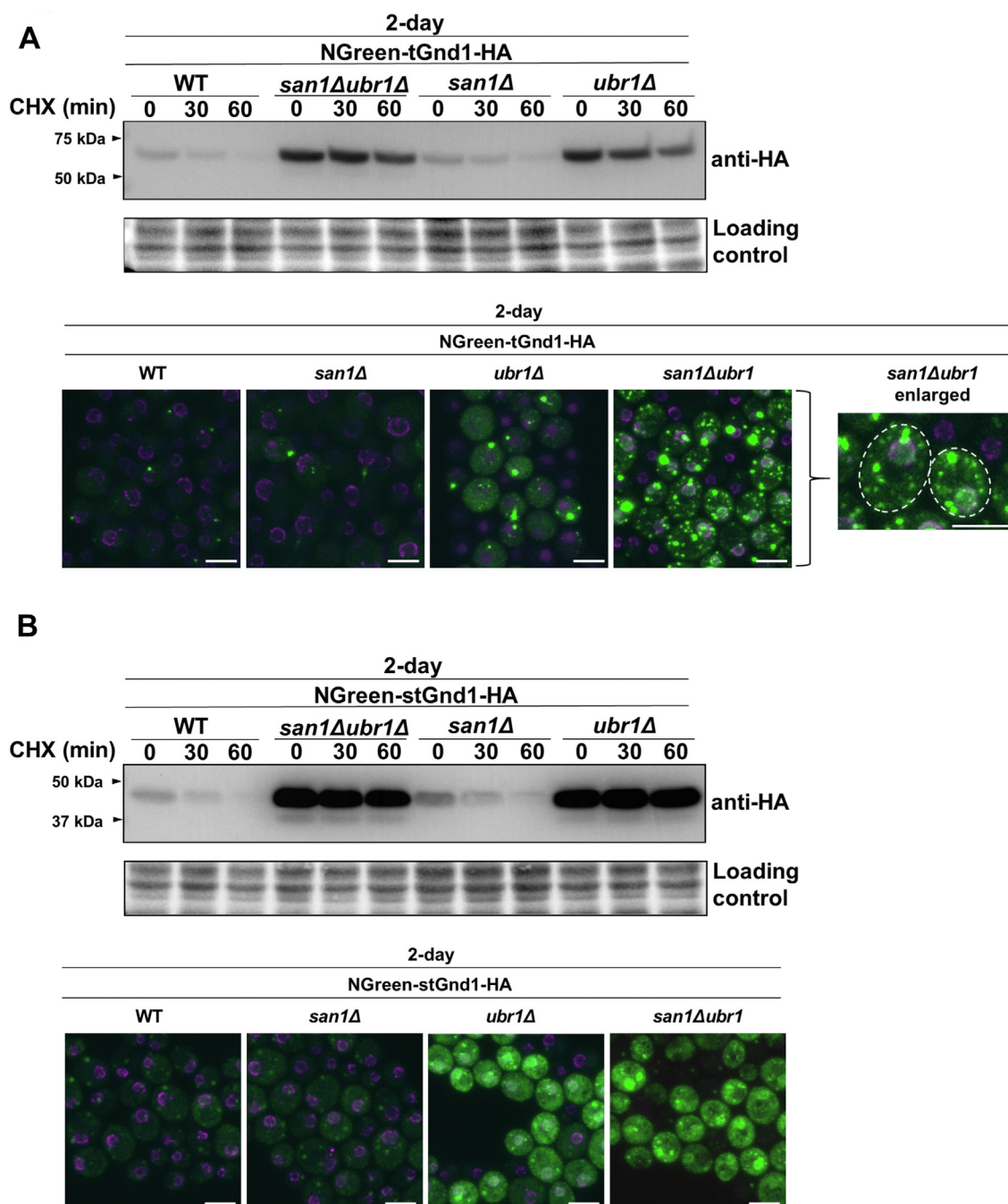


**Figure 3. tGnd1 expressed in quiescent cells of ubiquitination mutants forms inclusions, whereas stGnd1 retains a predominantly diffuse localization.** Immunoblot and localization of NGreen-tGnd1-HA (A) and NGreen-stGnd1-HA (B) in quiescent cells. NGreen-tGnd1-HA was expressed in 2-days cell cultures under the constitutive *PIR3*-promoter in wild type BY4741 (DFY192) and deletion mutants *san1Δ* (DFY193), *ubr1Δ* (DFY194), and *ubr1Δ san1Δ* (DFY195). NGreen-stGnd1-HA was similarly expressed in wild type (DFY196), *san1Δ* (DFY197), *ubr1Δ* (DFY198), and *ubr1Δ san1Δ* (DFY200). Cycloheximide chase analysis was performed as described in Figure 1. Stain-free total protein (Bio-Rad) was used as a loading control. Protein localization of the same cultures as in A was analyzed by confocal fluorescent microscopy. The green signal represents green fluorescent protein ymNeonGreen (NGreen), while red signal represents nucleoporin Nup49-mScarlet. Shown is the whole z-stack. Scale bar measures 10  $\mu$ m.

interactions between the vacuolar membrane protein Vac8 and the outer nuclear membrane protein Nvj1, whose size and frequency increases upon starvation (49, 50). To test the possibility that the clearance of misfolded proteins in quiescent cells involves nucleus-vacuole junctions, we examined the stability of tGnd1 and stGnd1 in the *nvj1Δ* and *vac8Δ* mutants, which are unable to form NVJ (49). The degradation of

tGnd1 was clearly impaired in the quiescent cells of the *nvj1Δ* and *vac8Δ* mutants, indicating a critical role of the NVJ in the clearance of tGnd1 (Fig. 6A). In contrast, the degradation of stGnd1 was not affected by the NVJ mutants (Fig. 6A). Considering the localization of tGnd1, but not stGnd1, to the inclusions, our data are consistent with a previous study (24) showing the localization of INQ/JUNQ in the vicinity of the

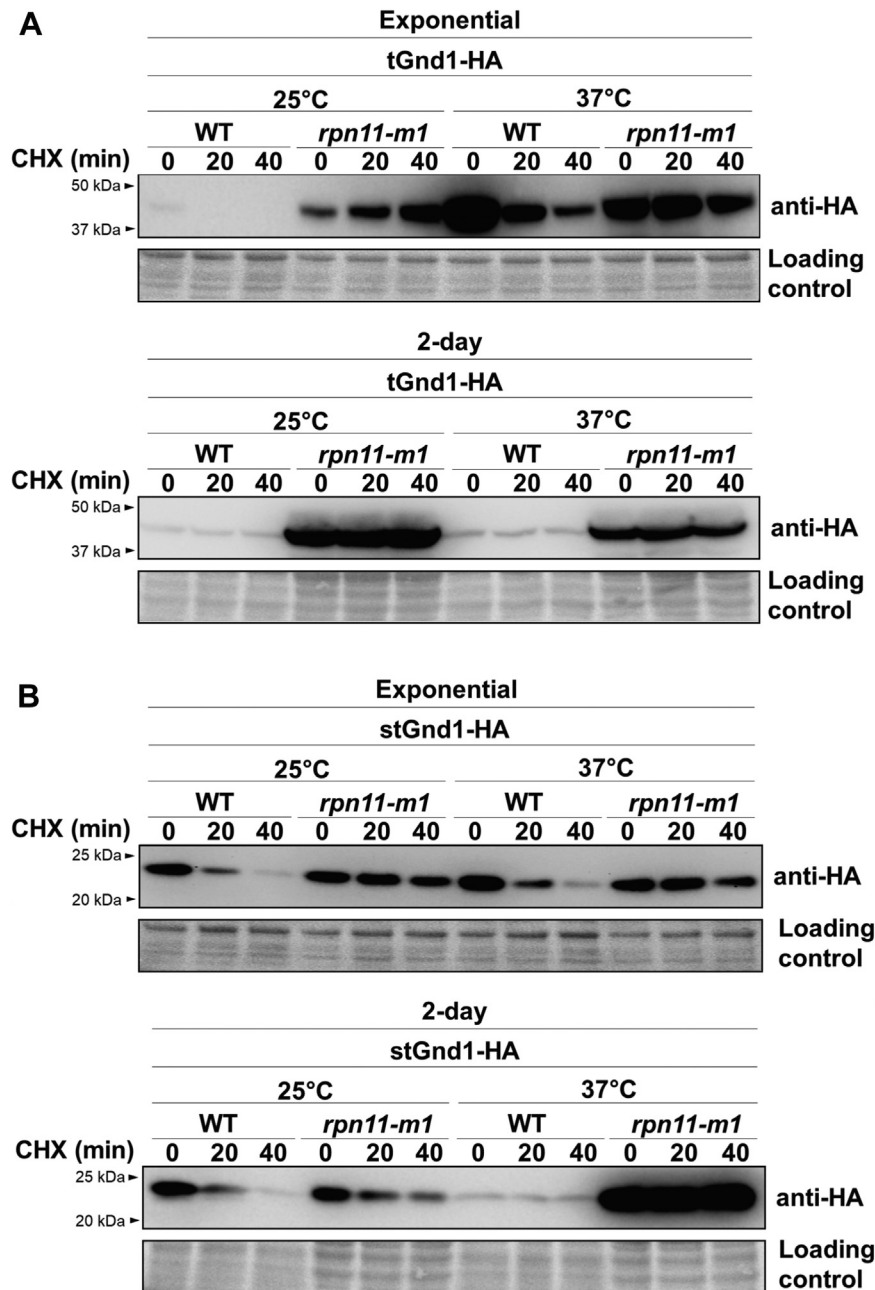


**Figure 4. The degradation of misfolded proteins tGnd1 and stGnd1 in quiescent cells is dependent on the activity of the proteasome.** Stability of tGnd1-HA and stGnd1-HA was assessed in the temperature-sensitive proteasome mutant strain *rpn11-m1*. Cell cultures were grown at permissive temperature of 25 °C to the exponential phase or for 2 days, then shifted to a restrictive temperature of 37 °C for 30 min, followed by cycloheximide chase and Western blot analysis as described in Figure 1. tGnd1-HA (A) and stGnd1-HA (B) were expressed from centromeric plasmids under the control of *TEF1*-promoter (pMB214, pMB215) or *PIR3*-promoter (pMB211, pMB212) in the wild type (W303) and *rpn11-m1* mutant (YP337). Stain-free total protein (Bio-Rad) was used as a loading control.

NVJ and the delivery of the INQ/JUNQ-localized misfolded proteins to the vacuole. Importantly, in our experiments, neither tGnd1 nor stGnd1 exhibited a detectable stabilization in the exponentially growing cells of the *nvj1Δ* and *vac8Δ* mutants (Fig. 6A), suggesting that the role of NVJ in the clearance of misfolded proteins becomes prominent upon cell entry into quiescence.

The stabilization of tGnd1 in the quiescent cells of the *vac8Δ* mutant was significantly stronger than in the *nvj1Δ* mutant. This data indicated that the loss of Vac8 leads to the

impairment of an additional pathway that is involved in tGnd1 degradation. Vac8 has been shown to be required for both bulk and selective autophagy (51–53). To test whether the clearance of tGnd1 via NVJ-dependent degradation and autophagy represent two separate pathways, we compared tGnd1 degradation in the single *nvj1Δ* mutant and a double *nvj1Δ atg1Δ* mutant and examined whether the double *nvj1Δ atg1Δ* mutant results in an additive effect. The stabilization of tGnd1 was considerably higher in the *nvj1Δ atg1Δ* double mutant, than in the single *nvj1Δ* mutant (Fig. 6B), demonstrating an



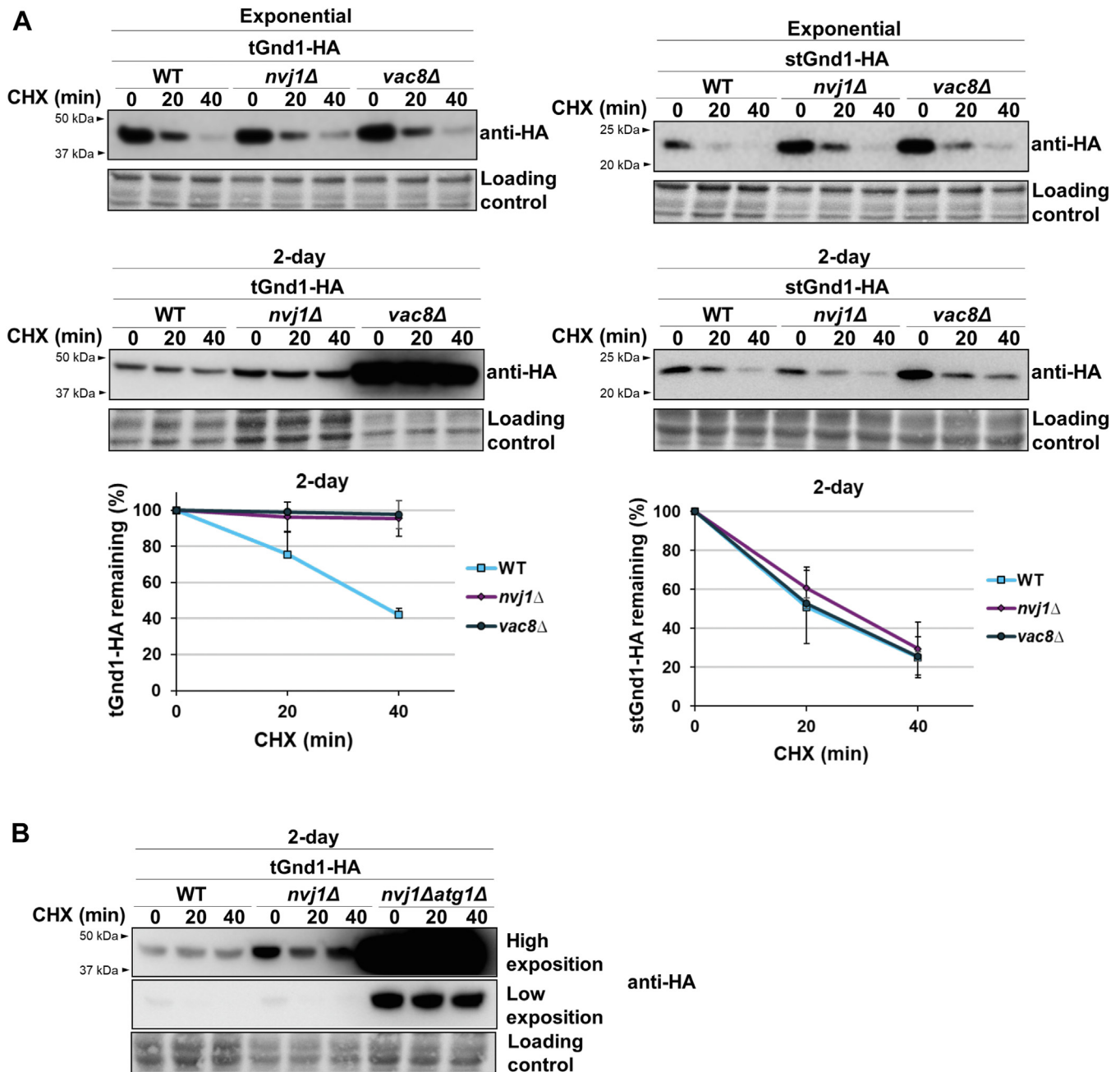


**Figure 6. Misfolded protein tGnd1 is stabilized in the nucleus-vacuole junction mutant *nvj1Δ*, and double mutation *nvj1Δ atg1Δ* leads to an additive effect.** Western blot analysis of the cycloheximide chase. *A*, cells expressing tGnd1-HA or stGnd1-HA under the control of *TEF1*-promoter (exponentially growing culture) or *PIR3*-promoter (2-day old culture) in the wild type (MPY152, MPY153, MPY154, MPY155), *nvj1Δ* mutant (MPY156, MPY158, MPY160, MPY162), and *vac8Δ* mutant (MPY157, MPY159, MPY161, MPY163) were analyzed as in Figure 1. *B*, the stability of tGnd1-HA was compared in the 2-day-old cultures from single *nvj1Δ* (MPY156) and double *nvj1Δ atg1Δ* (MPY164) mutant. Stain-free total protein (Bio-Rad) was used as a loading control. Graphs represent tGnd1-HA and stGnd1-HA protein levels as a percentage of the protein present at the time point 0 min. Average values and standard deviation are shown (n = 2).

additive effect of impaired autophagy and disrupted NVJ. The data indicate that NVJ-dependent clearance and autophagy represent two separate pathways in the degradation of tGnd1, and suggest that the two pathways operate in parallel.

### Discussion

This study shows that quiescent yeast cells retain degradation-mediated protein quality control, employing a combination of different pathways to mitigate the

accumulation of misfolded proteins. Despite the previously reported relocalization of proteasomes in quiescent cells, our data indicate that a significant pool of fully assembled and active 26S proteasomes are engaged in the degradation of quality control substrates. Moreover, in contrast to the exponentially growing cells, the efficient clearance of certain substrates necessitates the presence of intact nucleus-vacuole junctions and autophagy, which is independent of the only known ubiquitin-binding autophagy receptor in yeast, Cue5.

## Protein quality control in quiescence

Previous reports of the proteasomal substrates of the N-end rule (54) and ubiquitin fusion degradation (UFD) (55) pathways that were expressed in cells from stationary phase cultures suggested that the substrate degradation in quiescent cells was greatly decreased (41) or even abolished (39). However, due to the hardly detectable expression of the model substrates under the examined conditions (39), the interpretation was difficult. Furthermore, an earlier study of cells from stationary phase culture showed that a thermo-sensitive luciferase mutant formed inclusions, which suggested that quiescent cells may manage misfolded proteins primarily by sequestration (40). However, the role of degradation-mediated PQC in this process was not investigated. In our study, we expressed model misfolded proteins from the constitutive and inducible promoters that are active in quiescent cells and showed that misfolded proteins are targeted for selective degradation, in both early and later phases of cell quiescence.

A recent study has reported that the yeast strain BY4741 is unable to enter quiescence from the rich medium (56). In that study, BY4741 ceased dividing several hours before glucose exhaustion and the cell density reached a plateau at a low cell density ( $OD_{600} < 10$ ), already at 20 h post-inoculation. This was in contrast to the yeast strain W303, which did not exhibit such a phenotype (56). In our experiments, BY4741 continued to grow after glucose exhaustion, reaching a high cell density by the fourth day post-inoculation ( $OD_{600}$  above 40). The discrepancy may be attributed to the differences in the composition of the growth media. We have performed the key experiments in the W303 strain background. The results demonstrated that misfolded proteins *s/tGnd1* were degraded in W303 in a proteasome-dependent manner and that *tGnd1* was stabilized in an autophagy mutant (Figs. 4 and S3, respectively), indicating that active degradation pathways are present in the W303 strain, in a manner similar to those observed in BY4741-derived strains.

In quiescent cells, proteasomes relocate to the nuclear periphery and to cytoplasmic storage granules (37), which are thought to contain disassembled, inactive proteasomes (38, 39). Here we showed that the efficient removal of the misfolded protein *stGnd1* in quiescent cells was *Rpn11*-dependent, and did not require other pathways, such as autophagy or NVJ-mediated clearance. This finding supports the presence of fully assembled and functionally active 26S proteasomes in quiescent cells, and is consistent with a previous report showing that assembled 26S proteasomes were still detectable in quiescent cells (37). Our results indicate that 26S proteasomes are actively involved in the degradation of misfolded proteins in quiescent cells, suggesting that the pool of the proteasomes that is not integrated into proteasome storage granules is sufficient to meet the demand for PQC during quiescence, a state characterized by downregulation of new protein synthesis, and thus a lower burden of misfolded proteins.

Our results demonstrated that *tGnd1*, but not *stGnd1*, was stabilized in quiescent cells of autophagy mutants (Fig. 5, A–C), indicating selectivity. Inactivation of the only known

ubiquitin-binding autophagy receptor in yeast, *Cue5*, had no effect on *tGnd1* stability (Fig. 5D), suggesting that a distinct mechanism is involved. The sequestration of *tGnd1*, but not *stGnd1*, into the inclusions suggests that autophagy selectivity may be contingent upon *tGnd1* localization to the inclusions, a possibility that deserves further investigation, including the analysis of the additional substrates. A recent report has shown *Cue5*-independent autophagy of a poly-glutamine expanded huntingtin (*HttQ103*) protein expressed in dividing yeast cells (57). The process was termed inclusion body autophagy or IBophagy, and was dependent on the selective autophagy receptors *Atg36*, *Atg39* and *Atg40* (57). It is possible that a similar process is involved in the degradation of *tGnd1* in quiescent cells.

In our experiments *tGnd1* was clearly stabilized in the nucleus-vacuole junctions (NVJ) mutants, but only in quiescent cells (Fig. 6A). This finding is also consistent with a previous study that has demonstrated an increase in the frequency and size of the NVJ upon prolonged growth in YPD (50). The lack of *tGnd1* stabilization in the NVJ mutants of the exponentially growing cells suggests that the role of the NVJ-mediated clearance becomes critical in cell quiescence, presumably due to the limits in the proteasomal degradation of certain substrates.

Notably, *tGnd1* exhibited stabilization in the autophagy- and NVJ-mutants that had a functional ubiquitin-proteasome system, suggesting that proteasomes, autophagy and NVJ-dependent clearance function in parallel. The finding that the clearance of *tGnd1* in quiescent cells additionally depends on autophagy and NVJ-dependent clearance suggests that the efficiency of proteasomal degradation of *tGnd1* in quiescent cells is limited. The observation that another substrate, *stGnd1*, did not require NVJ or autophagy for efficient clearance (Figs. 5C and 6A, respectively), strongly suggests that the proteasomes themselves are not the limiting factor. Rather, substrate-specific factors that are necessary to ensure the delivery of the protein to the proteasome may be affected.

Our results suggest that quiescent cells utilize similar *Ubr1*- and *San1*-dependent ubiquitination pathways for tagging misfolded proteins for degradation as exponentially growing cells. The observed activity of *Ubr1* in quiescent cells is also consistent with an earlier observation of increased steady-state levels of a model misfolded protein  $\Delta ssCL^*myc$  in *ubr1Δ* mutant cells from stationary phase cultures (58). Of note, in quiescent cells, the degradation of *tGnd1* was more dependent on *Ubr1* than on *San1*. This is in contrast to exponentially growing cells in which *San1* had a similar contribution as *Ubr1* (Fig. 2A). This finding suggests that in quiescent cells, the delivery of *tGnd1* to *San1* for ubiquitination may be impaired, potentially due to an inability to transport *tGnd1* into the nucleus, or a lack of chaperones.

In support of the possibility that degradation of *tGnd1* in quiescent cells is limited by the availability of chaperones, the efficient degradation of *tGnd1* in exponentially growing cells has been shown to require Hsp40 chaperone *Sis1*, whereas *stGnd1* degradation was largely *Sis1*-independent (59). *Sis1*

**Table 1**  
Yeast strains used in this study

Yeast strain	Genotype	Reference
W303	<i>MATa; leu2-3112; trp1-1; can1-100; ura3-1; ade2-1; his3-11,15; phi+</i>	(70)
YP337	<i>MATa; his3Δ-200; ade2-101; leu2Δ1; ura3-52; lys2-801; trp1-62; YFR004W::rpn11-m1</i>	(70)
BY4741	<i>MATa; his3Δ1; leu2Δ0; met15Δ0; ura3Δ0</i>	Euroscarf (Germany)
Y00253	<i>his3Δ1; leu2Δ0; met15Δ0; ura3Δ0; vac8Δ::kanMX4</i>	Euroscarf (Germany)
Y01818	<i>his3Δ1; leu2Δ0; met15Δ0; ura3Δ0; cue5Δ::kanMX4</i>	Euroscarf (Germany)
Y04547	<i>his3Δ1; leu2Δ0; met15Δ0; ura3Δ0; atg1Δ::kanMX4</i>	Euroscarf (Germany)
Y03104	<i>his3Δ1; leu2Δ0; met15Δ0; ura3Δ0; atg8Δ::kanMX4</i>	Euroscarf (Germany)
Y02889	<i>his3Δ1; leu2Δ0; met15Δ0; ura3Δ0; nvj1Δ::kanMX4</i>	Euroscarf (Germany)
Y04077	<i>ura3Δ0; leu2Δ0; his3Δ1; met15Δ0; san1Δ::kanMX</i>	Euroscarf (Germany)
Y04814	<i>ura3Δ0; leu2Δ0; his3Δ1; met15Δ0; ubr1Δ::kanMX</i>	Euroscarf (Germany)
γTB281	<i>his3Δ1; leu2Δ0; ura3Δ0; met15Δ0; GFP-ATG8</i>	(71)
γTB293	<i>his3Δ1; leu2Δ0; ura3Δ0; met15Δ0; atg1Δ::KAN; GFP-ATG8</i>	(71)
DFY001	<i>MATa; his3Δ1; leu2Δ0; met15Δ0; ura3Δ0::PPIR- tGnd1-HA URA3</i>	This study
DFY002	<i>MATa; his3Δ1; leu2Δ0; met15Δ0; ura3Δ0::PPIR3-stGnd1-HA URA3</i>	This study
DFY003	<i>MATa; his3Δ1; leu2Δ0; met15Δ0; ura3Δ0::PPIR- Gnd1-HA URA3</i>	This study
DFY004	<i>MATa; his3Δ1; leu2Δ0; met15Δ0; ura3Δ0::PTEF1-tGnd1-HA URA3</i>	This study
DFY005	<i>MATa his3Δ1 leu2Δ0 met15Δ0 ura3Δ0::PTEF1-stGnd1-HA URA3</i>	This study
DFY006	<i>MATa his3Δ1 leu2Δ0 met15Δ0 ura3Δ0::PTEF1-Gnd1-HA URA3</i>	This study
DFY037	<i>MATa; his3Δ1; leu2Δ0; met15Δ0; ura3Δ0::PPIR3- tGnd1-HA, URA3; san1Δ::kanMX4</i>	This study
DFY038	<i>MATa; his3Δ1; leu2Δ0; met15Δ0; ura3Δ0::PPIR3-stGnd1-HA, URA3; san1Δ::kanMX4</i>	This study
DFY039	<i>MATa; his3Δ1; leu2Δ0; met15Δ0; ura3Δ0::PTEF1-tGnd1-HA, URA3; san1Δ::kanMX4</i>	This study
DFY040	<i>MATa; his3Δ1; leu2Δ0; met15Δ0; ura3Δ0::PTEF1-stGnd1-HA, URA3; san1Δ::kanMX4</i>	This study
DFY041	<i>MATa; his3Δ1; leu2Δ0; met15Δ0; ura3Δ0:: PPIR3-tGnd1-HA, URA3; ubr1Δ::kanMX4</i>	This study
DFY042	<i>MATa; his3Δ1; leu2Δ0; met15Δ0; ura3Δ0:: PPIR3-stGnd1-HA, URA3; ubr1Δ::kanMX4</i>	This study
DFY043	<i>MATa; his3Δ1; leu2Δ0; met15Δ0; ura3Δ0:: PTEF1-tGnd1-HA, URA3; ubr1Δ::kanMX4</i>	This study
DFY044	<i>MATa; his3Δ1; leu2Δ0; met15Δ0; ura3Δ0:: PTEF1-stGnd1-HA, URA3; ubr1Δ::kanMX4</i>	This study
DFY049	<i>MATa; his3Δ1; leu2Δ0; met15Δ0; ura3Δ0:: PPIR3-prog-inducible synTA-Zif268 DBD</i>	This study
DFY050	<i>MATa; his3Δ1; leu2Δ0; met15Δ0; ura3Δ0; san1Δ::kanMX4; ubr1Δ::hphMX</i>	This study
DFY052	<i>MATa his3Δ1:: pZ-tGnd1-HA, leu2Δ0 met15Δ0 ura3Δ0:: PPIR3-prog-inducible synTA-Zif268 DBD</i>	This study
DFY053	<i>MATa his3Δ1:: pZ-stGnd1-HA, leu2Δ0 met15Δ0 ura3Δ0:: PPIR3-prog-inducible synTA-Zif268 DBD</i>	This study
DFY054	<i>MATa his3Δ1:: pZ-Gnd1-3HA, leu2Δ0 met15Δ0 ura3Δ0:: PPIR3-prog-inducible synTA-Zif268 DBD</i>	This study
DFY055	<i>MATa; his3Δ1; leu2Δ0; met15Δ0; ura3Δ0:: PPIR3-tGnd1-HA; san1Δ::kanMX4; ubr1Δ::hphMX</i>	This study
DFY056	<i>MATa; his3Δ1; leu2Δ0; met15Δ0; ura3Δ0:: PPIR3-stGnd1-HA; san1Δ::kanMX4; ubr1Δ::hphMX</i>	This study
DFY057	<i>MATa; his3Δ1; leu2Δ0; met15Δ0; ura3Δ0:: PTEF1-tGnd1-HA; san1Δ::kanMX4; ubr1Δ::hphMX</i>	This study
DFY058	<i>MATa; his3Δ1; leu2Δ0; met15Δ0; ura3Δ0:: PTEF1-stGnd1-HA; san1Δ::kanMX4; ubr1Δ::hphMX</i>	This study
DFY115	<i>MATa his3Δ1, leu2Δ0 met15Δ0 ura3Δ0:: PPIR3-prog-inducible synTA-Zif268 DBD; san1Δ::kanMX4</i>	This study
DFY116	<i>MATa his3Δ1, leu2Δ0 met15Δ0 ura3Δ0:: PPIR3-prog-inducible synTA-Zif268 DBD; ubr1Δ::kanMX4</i>	This study
DFY117	<i>MATa his3Δ1, leu2Δ0 met15Δ0 ura3Δ0:: PPIR3-prog-inducible synTA-Zif268 DBD; san1Δ::kanMX4; ubr1Δ::hphMX</i>	This study
DFY118	<i>MATa his3Δ1:: pZ-tGnd1-HA, leu2Δ0 met15Δ0 ura3Δ0:: PPIR3-prog-inducible synTA-Zif268 DBD; san1Δ::kanMX4</i>	This study
DFY119	<i>MATa his3Δ1:: pZ-tGnd1-3HA, leu2Δ0 met15Δ0 ura3Δ0:: PPIR3-prog-inducible synTA-Zif268 DBD; ubr1Δ::kanMX4</i>	This study
DFY120	<i>MATa his3Δ1:: pZ-tGnd1-3HA, leu2Δ0 met15Δ0 ura3Δ0:: PPIR3-prog-inducible synTA-Zif268 DBD; san1Δ::kanMX4; ubr1Δ::hphMX</i>	This study
DFY121	<i>MATa his3Δ1:: pZ-stGnd1-3HA, leu2Δ0 met15Δ0 ura3Δ0:: PPIR3-prog-inducible synTA-Zif268 DBD; san1Δ::kanMX4</i>	This study
DFY122	<i>MATa his3Δ1:: pZ-stGnd1-3HA, leu2Δ0 met15Δ0 ura3Δ0:: PPIR3-prog-inducible synTA-Zif268 DBD; ubr1Δ::kanMX4</i>	This study
DFY123	<i>MATa his3Δ1:: pZ-stGnd1-3HA, leu2Δ0 met15Δ0 ura3Δ0:: PPIR3-prog-inducible synTA-Zif268 DBD; san1Δ::kanMX4; ubr1Δ::hphMX</i>	This study
DFY192	<i>MATa; his3Δ1::PPIR3-NGreen-tGnd1-HA, HIS3; leu2Δ0; met15Δ0; ura3Δ0::Nup49-mScarlet, URA3</i>	This study
DFY193	<i>MATa; his3Δ1::PPIR3-NGreen-tGnd1-HA, HIS3; leu2Δ0; met15Δ0; ura3Δ0::Nup49-mScarlet, URA3; san1Δ::kanMX4</i>	This study
DFY194	<i>MATa; his3Δ1::PPIR3-NGreen-tGnd1-HA, HIS3; leu2Δ0; met15Δ0; ura3Δ0::Nup49-mScarlet, URA3; ubr1Δ::kanMX4</i>	This study
DFY195	<i>MATa; his3Δ1::PPIR3-NGreen-tGnd1-HA, HIS3; leu2Δ0; met15Δ0; ura3Δ0::Nup49-mScarlet; san1Δ::kanMX4; ubr1Δ::hphMX</i>	This study
DFY196	<i>MATa; his3Δ1::PPIR3-NGreen-stGnd1-HA, HIS3; leu2Δ0; met15Δ0; ura3Δ0::Nup49-mScarlet-URA3</i>	This study
DFY197	<i>MATa; his3Δ1::PPIR3-NGreen-stGnd1-HA, HIS3; leu2Δ0; met15Δ0; ura3Δ0::Nup49-mScarlet, URA3; san1Δ::kanMX4</i>	This study
DFY198	<i>MATa; his3Δ1::PPIR3-NGreen-stGnd1-HA, HIS3; leu2Δ0; met15Δ0; ura3Δ0::Nup49-mScarlet, URA3; ubr1Δ::kanMX4</i>	This study
DFY200	<i>MATa; his3Δ1::PPIR3-NGreen-tGnd1-HA, HIS3; leu2Δ0; met15Δ0; ura3Δ0::Nup49-mScarlet; san1Δ::kanMX4; ubr1Δ::hphMX</i>	This study
MBY482	<i>MATa; his3Δ1; leu2Δ0; met15Δ0; ura3Δ0::PPIR3-tGnd1-HA URA3, cue5Δ::kanMX4</i>	This study
MBY483	<i>MATa; his3Δ1; leu2Δ0; met15Δ0; ura3Δ0::PPIR3-tGnd1-HA URA3, atg1Δ::kanMX4</i>	This study

## Protein quality control in quiescence

**Table 1**—Continued

Yeast strain	Genotype	Reference
MBY484	<i>MATa; his3Δ1; leu2Δ0; met15Δ0; ura3Δ0::PPIR3-tGnd1-HA URA3, atg8Δ::kanMX4</i>	This study
MBY486	<i>MATa; his3Δ1; leu2Δ0; met15Δ0; ura3Δ0::PPIR3-stGnd1-HA URA3, cue5Δ::kanMX4</i>	This study
MBY487	<i>MATa; his3Δ1; leu2Δ0; met15Δ0; ura3Δ0::PPIR3-stGnd1-HA URA3, atg1Δ::kanMX4</i>	This study
MBY488	<i>MATa; his3Δ1; leu2Δ0; met15Δ0; ura3Δ0::PPIR3-stGnd1-HA URA3, atg8Δ::kanMX4</i>	This study
MBY501	<i>his3Δ1; leu2Δ0; ura3Δ0::PPIR3-tGnd1-HA URA3; met15Δ0; GFP-ATG8</i>	This study
MBY507	<i>his3Δ1; leu2Δ0; ura3Δ0::PPIR3-tGnd1-HA URA3; met15Δ0; GFP-ATG8, atg1::kanMX4</i>	This study
MBY513	<i>MATa; his3Δ1; leu2Δ0; met15Δ0; ura3Δ0::PPIR3-tGnd1-HA URA3</i>	This study
MBY514	<i>MATa; his3Δ1; leu2Δ0; met15Δ0; ura3Δ0::PPIR3-stGnd1-HA URA3</i>	This study
MPY152	<i>MATa; his3Δ1; leu2Δ0; met15Δ0; ura3Δ0::PPIR3-tGnd1-HA URA3</i>	This study
MPY153	<i>MATa; his3Δ1; leu2Δ0; met15Δ0; ura3Δ0::PPIR3-stGnd1-HA URA3</i>	This study
MPY154	<i>MATa; his3Δ1; leu2Δ0; met15Δ0; ura3Δ0::PTEF1-tGnd1-HA URA3</i>	This study
MPY155	<i>MATa his3Δ1 leu2Δ0 met15Δ0 ura3Δ0::PTEF1-stGnd1-HA URA3</i>	This study
MPY156	<i>MATa; his3Δ1; leu2Δ0; met15Δ0; ura3Δ0::PPIR3-tGnd1-HA URA3; nvj1Δ::kanMX4</i>	This study
MPY157	<i>MATa; his3Δ1; leu2Δ0; met15Δ0; ura3Δ0::PPIR3-tGnd1-HA URA3; vac8Δ::kanMX4</i>	This study
MPY158	<i>MATa; his3Δ1; leu2Δ0; met15Δ0; ura3Δ0::PPIR3-stGnd1-HA URA3; nvj1Δ::kanMX4</i>	This study
MPY159	<i>MATa; his3Δ1; leu2Δ0; met15Δ0; ura3Δ0::PPIR3-stGnd1-HA URA3; vac8Δ::kanMX4</i>	This study
MPY160	<i>MATa; his3Δ1; leu2Δ0; met15Δ0; ura3Δ0::PTEF1-tGnd1-HA URA3; nvj1Δ::kanMX4</i>	This study
MPY161	<i>MATa; his3Δ1; leu2Δ0; met15Δ0; ura3Δ0::PTEF1-tGnd1-HA URA3; vac8Δ::kanMX4</i>	This study
MPY162	<i>MATa; his3Δ1; leu2Δ0; met15Δ0; ura3Δ0::PTEF1-stGnd1-HA URA3; nvj1Δ::kanMX4</i>	This study
MPY163	<i>MATa; his3Δ1; leu2Δ0; met15Δ0; ura3Δ0::PTEF1-stGnd1-HA URA3; vac8Δ::kanMX4</i>	This study
MPY164	<i>MATa; his3Δ1; leu2Δ0; met15Δ0; ura3Δ0::PPIR3-tGnd1-HA URA3; nvj1Δ::kanMX4; atg1Δ::hphMX</i>	This study
MPY166	<i>MATa/MATα; leu2-3112; trp1-1; can1-100; ura3-1:: PPIR3-tGnd1-HA, URA3; ade2-1; his3-11,15; phi+</i>	This study
MPY167	<i>MATa/MATα; leu2-3112; trp1-1; can1-100; ura3-1:: PPIR3-stGnd1-HA, URA3; ade2-1; his3-11,15; phi+</i>	This study
MPY170	<i>MATa/MATα; leu2-3112; trp1-1; can1-100; ura3-1:: PPIR3-tGnd1-HA, URA3; ade2-1; his3-11,15; phi+; atg1:: kanMX4</i>	This study

facilitates the delivery of misfolded proteins into the nucleus (59, 60) and nuclear substrate ubiquitination (15). Sis1 has also been implicated in Ubr1-mediated degradation (59), although its role in this process appears less prominent than its role in nuclear import. Additionally, a recent report demonstrated that the transition to respiratory metabolism and the accompanying decrease in translation rates in quiescent cells leads to the re-localization of protein disaggregase Hsp104 to the nucleus (61). It is plausible that the reduced levels of Hsp104 in the cytoplasm result in a lack of Hsp104 availability for the disaggregation of proteasomal substrates in the cytoplasm. Interestingly, stGnd1 was found slightly enriched in the nuclei of *ubr1Δ* and *san1Δ ubr1Δ* mutants (Fig. 3B). Since the wild-type strain exhibits very low stGnd1 protein levels, it is presently unclear whether nuclear access of stGnd1 is specific to the conditions of impaired protein degradation. The possibility that nuclear targeting of stGnd1 plays a role in stGnd1 solubilization and clearance, and the significance of nuclear localization for the protein quality control in quiescent cells require further investigation.

The data on PQC pathways in quiescent cells of mammalian organisms is limited. Proteasome foci have also been found in mammalian cells, where they form as a response to different types of stress, and in dendrites of neuronal cells (62), however, their presence in quiescent stem cells has not yet been investigated. A transcriptomic study of mouse neural stem cells has shown that activated neural stem cells exhibit increased expression of proteasome-associated genes, while quiescent neural stem cells exhibit increased expression of lysosome-associated genes, and have fewer catalytically active proteasomes (63). Quiescent neural stem cells accumulated insoluble protein aggregates, however, protein degradation has not been tested. In line with that, a study investigating dermal

fibroblasts showed that dermal fibroblasts increase the degradation rate of long-lived proteins upon entry into quiescence, by activating lysosome biogenesis and upregulating autophagy (64). Thus, autophagy upregulation upon cell cycle exit may be a common feature of quiescent cells in mammalian organisms. Collectively, the available data from mammalian organisms are in line with our results in yeast, which indicate that in addition to misfolded protein degradation *via* the ubiquitin-proteasome system, quiescent cells need functional autophagy to maintain protein homeostasis. Together, our findings underscore the importance of misfolded protein clearance during cell quiescence, and contribute to understanding the interplay of different degradation pathways.

### Experimental procedures

#### Yeast strains

Yeast *S. cerevisiae* strains used in this study are listed in Table 1. All strains used in this study were isogenic to BY4741 (65), except MPY166, *atg1Δ* mutant strain MPY170, and *rpn11-m1* mutant strain YP337, which were derived from W303. The description of strain construction is provided in Table 2. Strains were constructed by homologous recombination of DNA constructs or plasmids cut with the indicated restriction enzyme that were transformed into yeast strains. Molecular cloning was performed by standard methods. Sequences of all primers used in this study are listed in Table 3. Genome integration of the transformed DNA constructs was verified by PCR.

#### Yeast culture and growth media

Standard yeast culture media, such as ammonia-based synthetic complex dextrose (SC) medium containing 2% D-

**Table 2**  
Yeast strain construction

Yeast strain constructed	Construction	
	DNA used for transformation of the starting strain/restriction enzyme used to cut the DNA	Starting strain that was transformed with the indicated DNA
DFY001	pDF037/AscI	BY4741
DFY002	pDF038/AscI	BY4741
DFY003	pDF039/AscI	BY4741
DFY004	pDF040/AscI	BY4741
DFY005	pDF041/AscI	BY4741
DFY006	pDF042/AscI	BY4741
DFY037	pDF037/AscI	Y04077
DFY038	pDF038/AscI	Y04077
DFY039	pDF040/AscI	Y04077
DFY040	pDF041/AscI	Y04077
DFY041	pDF037/AscI	Y04814
DFY042	pDF038/AscI	Y04814
DFY043	pDF040/AscI	Y04814
DFY044	pDF041/AscI	Y04814
DFY049	pDF068/AscI	BY4741
DFY050	<i>ubr1</i> Δ::hphMX (PCR using pAG32)	Y04077
DFY052	pDF069/PmeI	DFY049
DFY053	pDF070/PmeI	DFY049
DFY054	pDF071/PmeI	DFY049
DFY055	pDF037/AscI	DFY050
DFY056	pDF038/AscI	DFY050
DFY057	pDF040/AscI	DFY050
DFY058	pDF041/AscI	DFY050
DFY115	pDF068/AscI	Y04077
DFY116	pDF068/AscI	Y04814
DFY117	pDF068/AscI	DFY050
DFY118	pDF069/PmeI	DFY115
DFY119	pDF069/PmeI	DFY116
DFY120	pDF069/PmeI	DFY117
DFY121	pDF070/PmeI	DFY115
DFY122	pDF070/PmeI	DFY116
DFY123	pDF070/PmeI	DFY117
DFY145	pDF037/AscI	MBY307
DFY146	pDF038/AscI	MBY307
DFY147	pDF040/AscI	MBY307
DFY148	pDF041/AscI	MBY307
DFY192	pDF129/PmeI, and PCR <i>NUP49</i> -mScarlet	BY4741
DFY193	pDF129/PmeI, and PCR <i>NUP49</i> -mScarlet	Y04077
DFY194	pDF129/PmeI, and PCR <i>NUP49</i> -mScarlet	Y04814
DFY195	pDF129/PmeI, and PCR <i>NUP49</i> -mScarlet	DFY050
DFY196	pDF128/PmeI, and PCR <i>NUP49</i> -mScarlet	BY4741
DFY197	pDF128/PmeI, and PCR <i>NUP49</i> -mScarlet	Y04077
DFY198	pDF128/PmeI, and PCR <i>NUP49</i> -mScarlet	Y04814
DFY200	pDF128/PmeI, and PCR <i>NUP49</i> -mScarlet	DFY050
MBY482	pDF037/AscI	Y01818
MBY483	pDF037/AscI	Y04547
MBY484	pDF037/AscI	Y03104
MBY486	pDF038/AscI	Y01818
MBY487	pDF038/AscI	Y04547
MBY488	pDF038/AscI	Y03104
MBY513	pDF037/AscI	BY4741
MBY514	pDF038/AscI	BY4741
MPY152	pDF037/AscI	BY4741
MPY153	pDF038/AscI	BY4741
MPY154	pDF040/AscI	BY4741
MPY155	pDF041/AscI	BY4741
MPY156	pDF037/AscI	Y02889
MPY157	pDF037/AscI	Y00253
MPY158	pDF038/AscI	Y02889
MPY159	pDF038/AscI	Y00253
MPY160	pDF040/AscI	Y02889
MPY161	pDF040/AscI	Y00253
MPY162	pDF041/AscI	Y02889
MPY163	pDF041/AscI	Y00253

**Table 2—Continued**

Yeast strain constructed	Construction	
	DNA used for transformation of the starting strain/restriction enzyme used to cut the DNA	Starting strain that was transformed with the indicated DNA
MPY164	<i>atg1</i> Δ::hphMX (PCR using pAG32)	MPY156
MPY166	pDF037/AscI	W303
MPY167	pDF038/AscI	W303
MPY170	<i>atg1</i> Δ::hphMX (PCR using pAG32)	MPY166

glucose were used. Yeast extract, peptone, dextrose (YPD) medium was prepared from 1% yeast extract (YEA03, Formedium Ltd.), 2% peptone (PEP03, Formedium Ltd.), and 2% D-glucose (GLU03, Formedium Ltd.). Antibiotic selections were made on solid YPD containing 200 mg/l G418 or 300 mg/l hygromycin B. When grown in liquid media, culture tubes and baffled flasks with loose-fitting caps were used, and cells were incubated in an orbital shaker (Innova 40R, New Brunswick) with shaking at 240 rpm. Cells were grown at 30 °C unless indicated otherwise. For the analysis of exponentially growing and quiescent cells, yeast overnight cultures were diluted in fresh YPD containing 2% glucose to an optical density OD<sub>600</sub> of 0.2 and grown to the exponential phase (OD<sub>600</sub> 0.8–1.0), or for a period of two to 7 days, as indicated, without media change. Where indicated, Z promoter was activated by the addition of progesterone (Sigma-Aldrich) to the media at the final concentration of 10 μM or 100 μM, as indicated, for 1 hour.

### Plasmids

All plasmids used in this study are listed in Table 4. The description of the plasmid construction is listed in Table 5. Sequences of primers used for construction are listed in Table 3.

### Measurement of glucose and ethanol concentration

Glucose concentration in the medium was determined using the Glucose (GO) Assay Kit (Sigma-Aldrich) following the manufacturer's instructions. Ethanol concentration was measured using a previously described protocol (66). Values of measurements of three independent samples are presented as mean values with standard deviations.

### Cell fractionation by centrifugation in density gradient

Cell fractionation in Percoll (Cytiva, Washington DC, USA) density gradient was performed as previously described (42). The gradient was prepared by mixing Percoll with 1.5 M NaCl in a 9:1 volume ratio, resulting in a total volume of 10 ml and a final NaCl concentration of 167 mM. To form the gradients, 1.8 ml of the Percoll solution was placed into 2 ml tubes and centrifuged (12,000 RPM, 15 min, 4 °C). Yeast overnight cultures were diluted in fresh YPD containing 2% glucose to an optical density OD<sub>600</sub> of 0.2 and grown for two or 5 days. A cell

## Protein quality control in quiescence

**Table 3**  
Primers used in this study

Primer	Sequence 5' → 3'	Purpose
prDF003	GTTGTTGGTACCGGTTTCTAAAATGTGCAACC	Cloning <i>PIR3</i> promoter
prDF004	TGTTGTTCTCGAGACTTATAAACAGTACTTGTTTATGAG	Cloning <i>PIR3</i> promoter
prDF050	GTGTTCTCGAGGTTGCTTAGGGACTTATAAACAGTACTTGTttatg	Cloning <i>PPiR3</i> (Avr1I)-s/tGnd1 constructs
prDF051	AGGAACCTAGGaatggtcttaagggtgaag	Cloning mNeonGreen-tagged s/tGnd1
prDF052	AGGAACCTCGAGACCAGAAAGACCACCACCACCAGAA CCctgtacaattcgtccatacc	Cloning mNeonGreen-tagged s/tGnd1
prKZ129	ACTGTTATGGATATCGCTGAGAGAAT CGCCGTGTACATCAAAAAACGAAAA CACTGGCATCATTGAGCATAATCCGT GAGGGTGCCTGGT	C-terminal tagging of Nup49 with mScarlet (Nup49-mScarlet)
prKZ130	TATCACACTATTAGCAATGACTTT CACATTTTAAAGGAAAATAATAGTA TTAAAAATTAACAGTGACGAAGG AAGGCAGCAGTATAGCGACCAGCAT	C-terminal tagging of Nup49 with mScarlet (Nup49-mScarlet)
prMB601	GTTGTTGGTACCACACACCATAGCTTCA	Construction of pMB151 (amplification of <i>PTEF1</i> )
prMB602	GTTGTTCTCGAGTTGTAATTAACCTTAGATTAG	Construction of pMB151 (amplification of <i>PTEF1</i> )
prMB603	GTTGTTCTAGATCATGTAATTAGTTATGTAC	Construction of pMB152 (amplification of <i>TCYC1</i> )
prMB604	GTTGTTGAGCTCGAAATTAAGCCTTCGAGCG	Construction of pMB152 (amplification of <i>TCYC1</i> )
prMB683	ATTTACATCAATAAGAAATCTCATAAAA CAAGTACTGTTTATAAGTCTCGAGATG TCTGCTGATTTCCGGTTG	Cloning <i>GND1</i> , <i>tGND1</i> and <i>stGND1</i>
prMB684	ACGTCATAGGGATAGCCCGCATAG TCAGGAACATCGTATGGGTATCTA GaACCAGCTTGGTATGTAGAGGAAG	Cloning <i>GND1</i>
prMB685	TTCTAGATACCCATACGATGTTCTGACTATGCGG	Cloning HA-epitope tag
prMB686	AACGTCATATGGATAGGATCCCTGCA TAGTCCGGGACGTCATAGGGATAG CCCGCATAGTCAGGAACATCGTATGG	Cloning HA-epitope tag
prMB687	TGCAGGATCCTATCCATATGACGTT CCAGATTACGCTTCTAGATGATGAA CTAGTTCTAGATCATGTAATTAGTT	Cloning HA-epitope tag
prMB688	GAGGGCGTGAATGTAAGCGTGACA TAACTAATTACATGATCTAGAACTAG	Cloning HA-epitope tag
prMB689	ACGTCATAGGGATAGCCCGCATAGT CAGGAACATCGTATGGGTATCTAGa ACCTGGCCAAGCTTCTCAGAAC	Cloning <i>stGND1</i>
prMB690	ACGTCATAGGGATAGCCCGCATAGTC AGGAACATCGTATGGGTATCTAGaA CCTCTAATGATACAACCACCTC	Cloning <i>tGND1</i>
prMB718f	GTTGTTctcgagaataaaGCACGAactagt GGTtCTAGATACCCATACGATGTTCC TGACTATGCGTGATAAccgeggAACAAc	Construction of plasmid with 3HA for protein tagging
prMB718r	GTTGTTccgeggTTATCACGCATAGTC AGGAACATCGTATGGGTATCTAGa ACCactagtTCGTGCTttattctcgagAACAAc	Construction of plasmid with 3HA for protein tagging
prMB753	GTTGTTGAATTCGCAGGCTAGCAATAAAATG	ZF/GAL4-DBD-progest.-TA
prMB755	GTTGTTACTAGTCGTATATAATTTAGCTATTTGCTTA	ZF/GAL4-DBD-progest.-TA
prMB848	AGAACGGTGACGATTACATTATCC	<i>CPS1</i> (forward)
prMB849	ACCAGTAGTCACATAGAACTCTTCG	<i>CPS1</i> (reverse)
prMB1019	ATCCTTCCGCTTCTGATTCTTC	<i>SANI</i> (forward)
prMB1020	GCTCTTAGTCTGTGTGGTGAG	<i>SANI</i> (reverse)
prMB1023	TACCAAACCTCCTTCCAAAC	<i>UBR1</i> (forward)
prMB1024	CGGTGTCATATCACGACATTCT	<i>UBR1</i> (reverse)

culture volume corresponding to 36 OD<sub>600</sub> units of cells was harvested by centrifugation (3000g, 3 min), resuspended in 180 µl 50 mM Tris buffer, and overlaid onto the preformed Percoll density gradient in 2 ml tubes. Cells were centrifuged in Percoll density gradient (400g for 60 min at 20 °C). Cell fractions were collected by pipetting, washed in 8 ml of Tris-buffer, and resuspended in 1 ml Tris-buffer. The optical density (OD<sub>600</sub>) of each cell fraction was measured, and a volume corresponding to 1 OD<sub>600</sub> units of cells was pelleted. Protein extraction and analysis by Western blot was performed as described below.

### Cycloheximide chase and Western blot analyses

Yeast overnight cultures were diluted in fresh YPD containing 2% glucose to an optical density OD<sub>600</sub> of 0.2 and grown to the exponential phase (OD<sub>600</sub> 0.8–1.0), or for a

period of two to 5 days, as indicated. Translation inhibitor cycloheximide (Sigma-Aldrich, St Louis, Missouri, USA) was added to the cell culture at a final concentration of 100 µg/ml. Cells were collected at the indicated time points following cycloheximide addition.

Total cell lysates were prepared as described (67) with some modifications. For the analysis of the proteins from exponentially growing cultures (OD<sub>600</sub> 0.8–1.0), 1.5 ml of cell culture was harvested. Cells were collected by centrifugation for (5 min, 11,000 RPM, 4 °C), the cell pellet was frozen in liquid nitrogen and stored at –20 °C until samples from all time points were collected. Protein isolation was done based on a previously described protocol (2) with some modifications. Briefly, cells were resuspended in 100 µl of ice-cold water, 100 µl of ice-cold 0.2 M NaOH was added, followed by incubation on ice for 10 min and centrifugation (5 min, 11,000

**Table 4**  
Plasmids used in this study

Plasmid	Description	Reference
pAG32	hphMX4, pFA6	(72)
pDF037	<i>PP1R3-tGnd1-HA, URA3</i> , integrative (based on pRG206MX)	This study
pDF038	<i>PP1R3-stGnd1-HA, URA3</i> , integrative (based on pRG206MX)	This study
pDF039	<i>PP1R3-Gnd1-HA, URA3</i> , integrative (based on pRG206MX)	This study
pDF040	<i>PTEF1-tGnd1-HA, URA3</i> , integrative (based on pRG206MX)	This study
pDF041	<i>PTEF1-stGnd1-HA, URA3</i> , integrative (based on pRG206MX)	This study
pDF042	<i>PTEF1-Gnd1-HA, URA3</i> , integrative (based on pRG206MX)	This study
pDF068	<i>PP1R3-prog-inducible synTA-Zif268 DBD, URA3</i> , integrative (based on pRG206MX)	This study
pDF069	pZ-tGnd1-HA, <i>HIS3</i> , integrative (based on pHES836)	This study
pDF070	pZ-stGnd1-HA, <i>HIS3</i> , integrative (based on pHES836)	This study
pDF071	pZ-Gnd1-HA, <i>HIS3</i> , integrative (based on pHES836)	This study
pDF072	<i>PP1R3 (AvrII) - tGND1-3HA, URA3</i> , integrative (based on pRG206MX)	This study
pDF073	<i>PP1R3 (AvrII) - stGND1-3HA, URA3</i> , integrative (based on pRG206MX)	This study
pDF126	<i>PP1R3-stGnd1-HA, HIS3</i> , integrative (based on pMB278)	This study
pDF127	<i>PP1R3-tGnd1-HA, HIS3</i> , integrative (based on pMB278)	This study
pDF128	<i>PP1R3-NeonGreen-stGnd1-HA HIS3</i> , integrative (based on pMB278)	This study
pDF129	<i>PP1R3-NeonGreen-tGnd1-HA HIS3</i> , integrative (based on pMB278)	This study
pFA6a-link-ymNeongreen-SpHis5	linker-ymNeonGreen (pFA6)	(43) gift from Bas Teusink (Addgene #125704)
pFA6a-link-ymScarlet1-URA3	linker-ymScarlet (pFA6)	(43) gift from Bas Teusink (Addgene #168055)
pMB151	<i>PTEF1, URA3, CEN</i> (based on pRG216)	This study
pMB152	<i>PTEF1-multicloning site -TCY1, URA3, CEN</i> (based on pRG216)	This study
pMB211	<i>PP1R3-tGnd1-HA, URA3, CEN</i> (based on pRG216)	This study
pMB212	<i>PP1R3-stGnd1-HA, URA3, CEN</i> (based on pRG216)	This study
pMB213	<i>PP1R3-Gnd1-HA, URA3, CEN</i> (based on pRG216)	This study
pMB214	<i>PTEF1-tGnd1-HA, URA3, CEN</i> (based on pRG216)	This study
pMB215	<i>PTEF1-stGnd1-HA, URA3, CEN</i> (based on pRG216)	This study
pMB216	<i>PTEF1-Gnd1-HA, URA3, CEN</i> (based on pRG216)	This study
pMB272	<i>PTEF1-multicloning site -TCY1, URA3</i> , integrative (based on pRG206MX)	This study
pMB274	<i>PTEF1-progesterone-induced ZifDBD-TA-TCY1, URA3</i> , integrative (based on pRG206MX)	This study
pMB278	pZ-multicloning site-HA tag, <i>HIS3</i> , integrative (based on pHES836)	This study
pHES830	<i>Zif268 DBD - hPR LBD - MSN2 AD, URA3</i> , integrative	(73) gift from Hana El-Samad (Addgene #87944)
pHES836	pZ-mKate2, <i>HIS3</i>	(73) gift from Hana El-Samad (Addgene #89195)
pRG206MX	<i>URA3</i> , integrative	(74) gift from Joerg Stelling (Addgene #64536)
pRG216	<i>URA3, CEN</i>	(74) gift from Joerg Stelling (Addgene #64536)
pXP732	<i>CYC1</i> terminator insert, <i>URA3, CEN</i>	(75) gift from Nancy DaSilva (Addgene #46058)

RPM at 4 °C). Cell pellets were resuspended in 50 µl SDS buffer (0.06 M Tris ± HCl, pH 6.8, 5% glycerol, 2% SDS, 4% β-mercaptoethanol, 0.0025% bromophenol blue), and incubated at 95 °C for 3 min. For the analysis of the proteins from density fractions isolated as above, the pellet was resuspended in 20 µL of SDS-buffer. Samples were centrifuged (5 min, 11,000 RPM at 23 °C) and the supernatant was kept. For the analysis of the proteins from quiescent cells (two- and five-day-old cultures), a cell culture volume corresponding to 10 OD<sub>600</sub> units of cells was harvested, and the same protocol as above was applied, but using double volumes of reagents, due to a larger number of cells (200 µl of distilled water, 200 µl of 0.2 NaOH, and 100 µl of SDS buffer).

Western blot was performed by antibodies: anti-HA (12CA5, Ogris laboratory, Max F. Perutz Laboratories, Vienna, Austria, 1/1000), anti-Pgk1 (22C5, RRID: AB\_2546088, Invitrogen 1/20,000), anti-GFP (Roche Diagnostics GmbH, Germany, 1/1000), and HRP-conjugated secondary antibodies Cell Signaling Technology, (#7076, 1/2000). The chemiluminescent signal intensity of immunoreactive bands was imaged by ChemiDoc MP Imaging System (BioRad Laboratories) and quantified by ImageLab (BioRad Laboratories). Stain-free signal of the total proteins (BioRad Laboratories) was used as a loading control. A

representative band of the stain-free signal is shown in the main figures, while full lanes are shown in Supporting Information Figs. S1 and S3–S9. Signal intensities of anti-HA-immunoreactive bands representing tGnd1-HA and stGnd1-HA were normalized to the Stain-free signal (BioRad Laboratories) of the total proteins originating from the whole lane. At least two independent samples were analyzed. Signal intensities are presented as mean values with standard deviations.

### Microscopy

Yeast overnight cultures were diluted in fresh YPD containing 2% glucose to an optical density OD<sub>600</sub> of 0.2 and grown for 2 days. Cells were fixed in 0.8% formaldehyde for 10 min, centrifuged, and washed twice in phosphate-buffered saline (PBS). The cell pellet was resuspended in PBS and dropped onto coverslips pre-coated with concanavalin-A (Sigma-Aldrich). Images were captured using a confocal fluorescent microscope Olympus FV3000 (Olympus) fitted with an Olympus-DP74 digital camera, an Olympus 60 × oil-immersion objective (Olympus UPlanSApo 60x/1.35 Oil Microscope Objective), and FV31S-SW Fluoview program. Figures were prepared using Fiji (ImageJ). The whole z-stack of the cells is shown.

## Protein quality control in quiescence

**Table 5**  
Plasmid construction

Plasmid	Description of the construction
pDF037 pDF038 pDF039 pDF040 pDF041 pDF042 pDF067	To obtain integrative plasmids, <i>PIR3</i> -tGND1-HA, <i>PIR3</i> -stGND1-HA and <i>PIR3</i> - <i>GND1</i> -HA constructs from pMB211, pMB212 and pMB213, respectively, were cut with KpnI and SpeI and ligated into pMB272 vector.
pDF068	To obtain integrative plasmids, tGND1-HA, stGND1-HA and GND1-HA constructs from CEN-plasmids pMB214, pMB215 and pMB216, respectively, were cut with XhoI and SpeI and the inserts were ligated into pMB272 vector, yielding pDF040, pDF041 and pDF042.
pDF069 pDF070 pDF071 pDF072	<i>TEF1</i> -promoter in pMB272 was exchanged to <i>PIR3</i> -promoter by ligating <i>PIR3</i> -promoter sequence into KpnI and XhoI-cut pMB272, yielding pDF067. <i>PIR3</i> -gene promoter had been PCR amplified from genomic DNA of wild-type BY4741 with primers prDF003 and prDF004.
pDF073	To place synthetic transcription factor (prog-inducible synTA-Zif268 DBD) under the control of <i>PIR3</i> -promoter, the insert was cut from pMB274 with EcoRI and SpeI, and ligated into similarly cut pDF067 vector containing <i>PIR3</i> -promoter.
pDF126 pDF127 pDF128 pDF129	To place tGND1-HA, stGND1-HA and GND1-HA constructs under the control of <i>Z</i> -promoter, pDF040, pDF041 or pDF042 plasmids were cut with XhoI/SacI and the inserts were ligated into pMB278, yielding pDF069, pDF070 and pDF071, respectively.
pMB151	<i>PIR3</i> containing an AvrII restriction site was amplified with primers pDF003 and 050 from pDF037, cut with XhoI and KpnI and ligated with similarly cut pDF037.
pMB152	<i>PIR3</i> containing an AvrII restriction site was amplified from pDF037 using primers pDF003 and 050, cut with XhoI/KpnI and ligated with similarly cut pDF038.
pMB211 pMB212 pMB213	<i>PIR3</i> -stGnd1-HA and <i>PIR3</i> -tGnd1-HA inserts were cut from plasmids pDF073 (stGnd1) and pDF072 (tGnd1), respectively, with KpnI/SacI, and ligated with similarly cut pMB278.
pMB214 pMB215 pMB216 pMB272	To insert mNeonGreen at the N-terminus of stGnd1-HA and tGnd1-HA, mNeonGreen was amplified from pFA6a-link-ymNeonGreen-SpHis5 using primers prDF051 and prDF052, cut with AvrII/XhoI and ligated with similarly cut pDF126 and pDF127, yielding pDF128 or pDF129, respectively.
pMB274	PCR product encompassing <i>TEF1</i> -promoter (obtained by primers prMB601, and prMB602 and genomic DNA of wild-type strain BY4742 as a template) was cut with KpnI and XhoI, and ligated with similarly cut pRG216 vector.
pMB275	PCR product encompassing <i>CYC1</i> -terminator (obtained by primers prMB603 and prMB604, and pXP732 as a template) was cut with XbaI and SacI and ligated with similarly cut pMB151 vector.
pMB276	Cloning of plasmids pMB211–213 was done in several steps. To clone pMB211, first, tGND1 missing codons for the last 121 amino acids was amplified by PCR from genomic DNA of BY4741 using primers prMB683 and prMB690, yielding DNA fragment “A-211”.
pMB277	To clone pMB212, first, stGND1 (missing codons for the last 339 amino acids) was cloned in several steps: was amplified by PCR from genomic DNA of BY4741 using primers prMB683 and prMB689, yielding DNA fragment “A-212”. To clone pMB213, first, <i>GND1</i> was amplified by PCR from genomic DNA of BY4741 using primers prMB683 and prMB684, yielding DNA fragment “A-213”.
	Second, 3HA cassette was assembled by annealing of oligonucleotides prMB685, 686, 687, 688 and amplified by PCR, yielding DNA fragment “B”.
	Third, DNA fragment “C” was XhoI/SpeI-cut vector containing <i>PIR3</i> and <i>TCYC1</i> , and a <i>URA3</i> selection marker.
	Finally, plasmids pMB211, pMB212 and pMB213 were created using homologous recombination, by co-transforming a Ura <sup>+</sup> yeast strain with the DNA fragments “A”, “B” and “C”, followed by selection for Ura <sup>+</sup> colonies.
	To place tGND1-HA, stGND1-HA or GND1-HA construct under the control of <i>TEF1</i> -promoter, the constructs were cut from pMB211, pMB212 or pMB213, respectively, by XhoI/SpeI, and ligated with similarly cut pMB152 vector.
	To obtain integrative <i>URA3</i> plasmid carrying PTEF1-linker- <i>TCYC1</i> construct, pMB152 was cut with EagI and this insert was ligated into EagI-cut pRG206MX vector.
	PCR product amplified from pHEs830 with prMB753 and prMB755 was cut with EcoRI and SpeI and ligated into pMB272 vector.
	3HA was amplified from pMB211 with primers prMB718-f and prMB718-r, cut with XhoI and SacII, and ligated into pHEs836 vector.

### mRNA analysis

Yeast overnight cultures were diluted in fresh YPD containing 2% glucose to an optical density OD<sub>600</sub> of 0.2 and grown to the exponential phase (OD<sub>600</sub> 0.8–1.0), or for a period of 2 days. Cells corresponding to 10 OD<sub>600</sub> were harvested by centrifugation at 4 °C, washed twice in ice-cold water, frozen in liquid nitrogen and stored at –80 °C until further processing. Total RNA was extracted using the hot phenol method (68) and purified with DNase I (RNase-free, New England Biolabs). DNase treatment was performed according to the manufacturer’s protocol with incubation at 37 °C for 10 min. RNA was then extracted with phenol/chloroform isoamyl alcohol (pH 6.7) and centrifuged at 10,000 rpm for 10 min at 4 °C. The aqueous phase was collected, followed by the addition of sodium acetate (pH 5.3) to a final concentration of 0.3 M and 3 volumes of 100% ethanol. Samples were precipitated at –80 °C for 20 min and centrifuged at 10,000 rpm for 10 min at 4 °C. RNA pellet was washed with 80% ethanol, centrifuged for 2 min at 10,000 rpm at 4 °C and air-dried at 30 °C. RNA was resuspended in 15 µl of RNase-free water, quantified using a Nanodrop spectrophotometer, and RNA integrity was assessed by 1% agarose gel

electrophoresis. RNA samples were stored at –80 °C. cDNA was synthesized using a High Capacity cDNA Reverse Transcription Kit (Applied Biosystems, Thermo Fisher Scientific) following the manufacturer’s protocol. qPCR was performed with Luna Universal qPCR Master Mix (New England Biolabs) using 100 ng of cDNA per reaction. Data were analyzed using the  $\Delta\Delta C_t$  method and relative expression levels were calculated as  $2^{-\Delta\Delta C_t}$ . The expression of *SANI* was analyzed using primers prMB1019 and prMB1020, and *UBR1* using primers prMB1023 and prMB1024 (sequences in Table 3). *CPS1* mRNA was used as the internal control for normalization (69), using primers prMB848 and prMB849 (Table 3). Relative expression levels of *SANI* and *UBR1* transcripts in cells from 2-day-old cultures were compared to those in exponentially growing cells. Two biological replicates were analyzed, and the analysis of each of those samples was performed in duplicates. Mean values of  $2^{-\Delta\Delta C_t}$  and standard deviation are shown.

### Statistical analysis

Values of an indicated number of independent samples analyzed were presented as mean values with standard deviations.

## Data availability

All data are contained within the manuscript.

**Supporting information**—This article contains supporting information.

**Acknowledgments**—Strains yTB281 and yTB293 were a kind gift from Claudine Kraft. Strains W303 and YP337 were a kind gift from Elah Pick. Plasmids pHES830 and pHES836 were a gift from Hana El-Samad, plasmids pRG206MX and pRG216 were a gift from Joerg Stelling, plasmid pXP732 was gift from Nancy Da Silva, and pFA6a-mScarlet was a gift from Bas Teusink, all via Addgene.

**Author contributions**—M. B., S. M., A. B., M. P., K. Z., and D. F. writing—review & editing; M. B., S. M., M. P., K. Z., and D. F. writing—original draft; M. B. and A. B. supervision; M. B. project administration; M. B., M. P., and D. F. methodology; M. B., S. M., M. P., K. Z., and D. F. investigation; M. B. funding acquisition; M. B. and A. B. conceptualization. S. M., M. P., K. Z., and D. F. validation; A. B. resources; A. B. formal analysis; M. P. and D. F. visualization.

**Funding and additional information**—This work was funded by the Research Cooperability Program of the Croatian Science Foundation, grant no. PZS-2019-02-3610 and DOK-2021-02-2505 to MB; by Croatian Science Foundation, grant no. IP-2022-10-6851; by the European Union through the European Regional Development Fund, Operational Program Competitiveness and Cohesion, grant agreement no. KK.01.1.1.01.0007, CoRE-Neuro, and by the National Institutes of Health (NIH, grant. no. R01 GM117446 to A. B.).

**Conflict of interest**—The authors declare that they have no conflicts of interest with the contents of this article.

**Abbreviations**—The abbreviations used are: INQ, intranuclear quality control compartment; JUNQ, juxtannuclear quality control compartment; NVJ, nucleus-vacuole junctions; PQC, protein quality control.

## References

- Hartl, F. U., Bracher, A., and Hayer-Hartl, M. (2011) Molecular chaperones in protein folding and proteostasis. *Nature* **475**, 324–332
- Balchin, D., Hayer-Hartl, M., and Hartl, F. U. (2016) In vivo aspects of protein folding and quality control. *Science* **353**, aac4354
- Needham, P. G., Guerriero, C. J., and Brodsky, J. L. (2019) Chaperoning endoplasmic reticulum-associated degradation (ERAD) and protein conformational diseases. *Cold Spring Harb Perspect. Biol.* **11**, a033928
- Pohl, C., and Dikic, I. (2019) Cellular quality control by the ubiquitin-proteasome system and autophagy. *Science* (1979) **366**, 818–822
- Douglas, P. M., and Dillin, A. (2010) Protein homeostasis and aging in neurodegeneration. *J. Cell Biol.* **190**, 719–729
- Finley, D., and Prado, M. A. (2020) The proteasome and its network: engineering for adaptability. *Cold Spring Harb Perspect. Biol.* **12**, a033985
- Sontag, E. M., Samant, R. S., and Frydman, J. (2017) Mechanisms and functions of spatial protein quality control. *Annu. Rev. Biochem.* **86**, 97–122
- Miller, S. B. M., Mogk, A., and Bukau, B. (2015) Spatially organized aggregation of misfolded proteins as cellular stress defense strategy. *J. Mol. Biol.* **427**, 1564–1574
- Ciechanover, A., and Stanhill, A. (2014) The complexity of recognition of ubiquitinated substrates by the 26S proteasome. *Biochim. Biophys. Acta* **1843**, 86–96
- Kriegenburg, F., Ellgaard, L., and Hartmann-Petersen, R. (2012) Molecular chaperones in targeting misfolded proteins for ubiquitin-dependent degradation. *FEBS J.* **279**, 532–542
- Heck, J. W., Cheung, S. K., and Hampton, R. Y. (2010) Cytoplasmic protein quality control degradation mediated by parallel actions of the E3 ubiquitin ligases Ubr1 and San1. *Proc. Natl. Acad. Sci.* **107**, 1106–1111
- Prasad, R., Kawaguchi, S., and Ng, D. T. W. (2010) A nucleus-based quality control mechanism for cytosolic proteins. *Mol. Biol. Cell* **21**, 2117–2127
- Nillegoda, N. B., Theodoraki, M. A., Mandal, A. K., Mayo, K. J., Ren, H. Y., Sultana, R., *et al.* (2010) Ubr1 and Ubr2 function in a quality control pathway for degradation of unfolded cytosolic proteins. *Mol. Biol. Cell* **21**, 2102–2116
- Maurer, M. J., Spear, E. D., Yu, A. T., Lee, E. J., Shahzad, S., and Michaelis, S. (2016) Degradation signals for ubiquitin-proteasome dependent cytosolic protein quality control (CytoQC) in yeast. *G3 (Bethesda)* **6**, 1853–1866
- Prasad, R., Xu, C., and Ng, D. T. W. (2018) Hsp40/70/110 chaperones adapt nuclear protein quality control to serve cytosolic clients. *J. Cell Biol.* **217**, 2019–2032
- Franić, D., Zubčić, K., and Boban, M. (2021) Nuclear ubiquitin-proteasome pathways in proteostasis maintenance. *Biomolecules* **11**, 54
- Samant, R. S., Livingston, C. M., Sontag, E. M., and Frydman, J. (2018) Distinct proteostasis circuits cooperate in nuclear and cytoplasmic protein quality control. *Nature* **563**, 407–411
- Borgert, L., Mishra, S., and den Brave, F. (2022) Quality control of cytoplasmic proteins inside the nucleus. *Comput. Struct. Biotechnol. J.* **20**, 4618–4625
- Collins, G. A., and Goldberg, A. L. (2017) The logic of the 26S proteasome. *Cell* **169**, 792–806
- Sahu, I., and Glickman, M. H. (2021) Proteasome in action: substrate degradation by the 26S proteasome. *Biochem. Soc. Trans.* **49**, 629–644
- Kaganovich, D., Kopito, R., and Frydman, J. (2008) Misfolded proteins partition between two distinct quality control compartments. *Nature* **454**, 1088–1095
- Miller, S. B., Ho, C., Winkler, J., Khokhrina, M., Neuner, A., Mohamed, M. Y., *et al.* (2015) Compartment-specific aggregates direct distinct nuclear and cytoplasmic aggregate deposition. *EMBO J.* **34**, 778–797
- Escusa-Toret, S., Vonk, W. I. M., and Frydman, J. (2013) Spatial sequestration of misfolded proteins by a dynamic chaperone pathway enhances cellular fitness during stress. *Nat. Cell Biol.* **15**, 1231–1243
- Sontag, E. M., Morales-Polanco, F., Chen, J.-H., McDermott, G., Dolan, P. T., Gestaut, D., *et al.* (2023) Nuclear and cytoplasmic spatial protein quality control is coordinated by nuclear–vacuolar junctions and perinuclear ESCRT. *Nat. Cell Biol.* **25**, 699–713
- Specht, S., Miller, S. B. M., Mogk, A., and Bukau, B. (2011) Hsp42 is required for sequestration of protein aggregates into deposition sites in *Saccharomyces cerevisiae*. *J. Cell Biol.* **195**, 617–629
- Malinowska, L., Kroschwald, S., Munder, M. C., Richter, D., and Alberti, S. (2012) Molecular chaperones and stress-inducible protein-sorting factors coordinate the spatiotemporal distribution of protein aggregates. *Mol. Biol. Cell* **23**, 3041–3056
- Den Brave, F., Cairo, L. V., Jagadeesan, C., Ruger-Herreros, C., Mogk, A., Bukau, B., *et al.* (2020) Chaperone-mediated protein disaggregation triggers proteolytic clearance of intra-nuclear protein inclusions. *Cell Rep.* **31**, 107680
- Bauer, B., Martens, S., and Ferrari, L. (2023) Aggrephagy at a glance. *J. Cell Sci.* **136**, jcs260888
- Yin, Z., Pascual, C., and Klionsky, D. J. (2016) Autophagy: machinery and regulation. *Microb. Cell.* **3**, 588–596
- Adriaenssens, E., Ferrari, L., and Martens, S. (2022) Orchestration of selective autophagy by cargo receptors. *Curr. Biol.* **32**, R1357–R1371
- Breeden, L. L., and Tsukiyama, T. (2022) Quiescence in *Saccharomyces cerevisiae*. *Annu. Rev. Genet.* **56**, 253–278
- Sagot, I., and Laporte, D. (2019) The cell biology of quiescent yeast - a diversity of individual scenarios. *J. Cell Sci.* **132**, jcs213025
- Montrose, K., López Cabezas, R. M., Paukštytė, J., and Saarikangas, J. (2020) Winter is coming: regulation of cellular metabolism by enzyme polymerization in dormancy and disease. *Exp. Cell Res.* **397**, 112383

## Protein quality control in quiescence

34. Miles, S., and Breeden, L. (2017) A common strategy for initiating the transition from proliferation to quiescence. *Curr. Genet.* **63**, 179–186
35. Werner-Washburne, M., Roy, S., and Davidson, G. S. (2011) Aging and the survival of quiescent and non-quiescent cells in yeast stationary-phase cultures. In Breitenbach, M., Jazwinski, S. M., Laun, P., eds., *Aging Research in Yeast 57*. Springer, Netherlands, Dordrecht: 123–143
36. Russell, S. J., Steger, K. A., and Johnston, S. A. (1999) Subcellular localization, stoichiometry, and protein levels of 26 S proteasome subunits in yeast. *J. Biol. Chem.* **274**, 21943–21952
37. Laporte, D., Salin, B., Daignan-Fornier, B., and Sagot, I. (2008) Reversible cytoplasmic localization of the proteasome in quiescent yeast cells. *J. Cell Biol.* **181**, 737–745
38. Li, J., Breker, M., Graham, M., Schuldiner, M., and Hochstrasser, M. (2019) AMPK regulates ESCRT-dependent microautophagy of proteasomes concomitant with proteasome storage granule assembly during glucose starvation. *PLoS Genet.* **15**, e1008387
39. Bajorek, M., Finley, D., and Glickman, M. H. (2003) Proteasome disassembly and downregulation is correlated with viability during stationary phase. *Curr. Biol.* **13**, 1140–1144
40. Lee, H.-Y., Chao, J.-C., Cheng, K.-Y., and Leu, J.-Y. (2018) Misfolding-prone proteins are reversibly sequestered to an Hsp42-associated granule upon chronological aging. *J. Cell Sci.* **131**, jcs220202
41. Paz, I., Meunier, J. R., and Choder, M. (1999) Monitoring dynamics of gene expression in yeast during stationary phase. *Gene* **236**, 33–42
42. Allen, C., Büttner, S., Aragon, A. D., Thomas, J. A., Meirelles, O., Jaetao, J. E., et al. (2006) Isolation of quiescent and nonquiescent cells from yeast stationary-phase cultures. *J. Cell Biol.* **174**, 89–100
43. Botman, D., de Groot, D. H., Schmidt, P., Goedhart, J., and Teusink, B. (2019) In vivo characterisation of fluorescent proteins in budding yeast. *Sci. Rep.* **9**, 2234
44. Rinaldi, T., Ricci, C., Porro, D., Bolotin-Fukuhara, M., and Frontali, L. (1998) A mutation in a novel yeast proteasomal gene, RPN11/MPRI, produces a cell cycle arrest, overreplication of nuclear and mitochondrial DNA, and an altered mitochondrial morphology. *Mol. Biol. Cell* **9**, 2917–2931
45. Iwama, R., and Ohsumi, Y. (2019) Analysis of autophagy activated during changes in carbon source availability in yeast cells. *J. Biol. Chem.* **294**, 5590–5603
46. Torggler, R., Papinski, D., and Kraft, C. (2017) Assays to monitor autophagy in *Saccharomyces cerevisiae*. *Cells* **6**, 23
47. Lu, K., Psakhye, I., and Jentsch, S. (2014) Autophagic clearance of PolyQ proteins mediated by ubiquitin-Atg8 adaptors of the conserved CUET protein family. *Cell.* **158**, 549–563
48. Lu, K., Den Brave, F., and Jentsch, S. (2017) Receptor oligomerization guides pathway choice between proteasomal and autophagic degradation. *Nat. Cell Biol.* **19**, 732–739
49. Pan, X., Roberts, P., Chen, Y., Kvam, E., Shulga, N., Huang, K., et al. (2000) Nucleus–vacuole junctions in *Saccharomyces cerevisiae* are formed through the direct interaction of Vac8p with Nvj1p. *Mol. Biol. Cell* **11**, 2445–2457
50. Roberts, P., Moshitch-Moshkovitz, S., Kvam, E., O’Toole, E., Winey, M., and Goldfarb, D. S. (2003) Piecemeal microautophagy of nucleus in *Saccharomyces cerevisiae*. *Mol. Biol. Cell* **14**, 129–141
51. Cheong, H., Yorimitsu, T., Reggiori, F., Legakis, J. E., Wang, C.-W., and Klionsky, D. J. (2005) Atg17 regulates the magnitude of the autophagic response. *Mol. Biol. Cell* **16**, 3438–3453
52. Hollenstein, D. M., Licheva, M., Konradi, N., Schweida, D., Mancilla, H., Mari, M., et al. (2021) Spatial control of avidity regulates initiation and progression of selective autophagy. *Nat. Commun.* **12**, 7194
53. Hollenstein, D. M., Gómez-Sánchez, R., Ciftci, A., Kriegenburg, F., Mari, M., Torggler, R., et al. (2019) Vac8 spatially confines autophagosome formation at the vacuole in *S. cerevisiae*. *J. Cell Sci.* **132**, jcs235002
54. Varshavsky, A. (1992) The N-end rule. *Cell* **69**, 725–735
55. Johnson, E. S., Ma, P. C., Ota, I. M., and Varshavsky, A. (1995) A proteolytic pathway that recognizes ubiquitin as a degradation signal. *J. Biol. Chem.* **270**, 17442–17456
56. Miles, S., Lee, C., and Breeden, L. (2023) BY4741 cannot enter quiescence from rich medium. *Micropubl Biol.* <https://doi.org/10.17912/micropub.biology.000742>
57. Folger, A., Chen, C., Kabbaj, M.-H., Frey, K., and Wang, Y. (2023) Neurodegenerative disease-associated inclusion bodies are cleared by selective autophagy in budding yeast. *Autophagy Rep.* **2**, 2236407
58. Amm, I., Norell, D., and Wolf, D. H. (2015) Absence of the yeast Hsp31 chaperones of the DJ-1 superfamily perturbs cytoplasmic protein quality control in late growth phase. *PLoS One* **10**, e0140363
59. Singh, A., Vashistha, N., Heck, J., Tang, X., Wipf, P., Brodsky, J. L., et al. (2020) Direct involvement of Hsp70 ATP hydrolysis in Ubr1-dependent quality control. *Mol. Biol. Cell* **31**, 2669–2686
60. Park, S.-H., Kukushkin, Y., Gupta, R., Chen, T., Konagai, A., Hipp, M. S., et al. (2013) PolyQ proteins interfere with nuclear degradation of cytosolic proteins by sequestering the Sis1p chaperone. *Cell.* **154**, 134–145
61. Kohler, V., Kohler, A., Berglund, L. L., Hao, X., Gersing, S., Imhof, A., et al. (2024) Nuclear Hsp104 safeguards the dormant translation machinery during quiescence. *Nat. Commun.* **15**, 315
62. Enenkel, C., Kang, R. W., Wilfling, F., and Ernst, O. P. (2022) Intracellular localization of the proteasome in response to stress conditions. *J. Biol. Chem.* **298**, 102083
63. Leeman, D. S., Hebestreit, K., Ruetz, T., Webb, A. E., McKay, A., Pollina, E. A., et al. (2018) Lysosome activation clears aggregates and enhances quiescent neural stem cell activation during aging. *Science* **359**, 1277–1283
64. Zhang, T., Wolfe, C., Pierle, A., Welle, K. A., Hryhorenko, J. R., and Ghaemmaghami, S. (2017) Proteome-wide modulation of degradation dynamics in response to growth arrest. *Proc. Natl. Acad. Sci. U. S. A.* **114**, E10329–E10338
65. Brachmann, C. B., Davies, A., Cost, G. J., Caputo, E., Li, J., Hieter, P., et al. (1998) Designer deletion strains derived from *Saccharomyces cerevisiae* S288C: a useful set of strains and plasmids for PCR-mediated gene disruption and other applications. *Yeast* **14**, 115–132
66. Miah, R., Siddiqua, A., Tuli, J. F., Barman, N. K., Dey, S. K., Adnan, N., et al. (2017) Inexpensive procedure for measurement of ethanol: application to bioethanol production process. *Adv. Microbiol.* **07**, 743–748
67. Kushnirov, V. V. (2000) Rapid and reliable protein extraction from yeast. *Yeast* **16**, 857–860
68. Schmitt, M. E., Brown, T. A., and Trumpower, B. L. (1990) A rapid and simple method for preparation of RNA from *Saccharomyces cerevisiae*. *Nucleic Acids Res.* **18**, 3091–3092
69. Nevers, A., Doyen, A., Malabat, C., Néron, B., Kergrohen, T., Jacquier, A., et al. (2018) Antisense transcriptional interference mediates condition-specific gene repression in budding yeast. *Nucleic Acids Res.* **46**, 6009–6025
70. Bramasole, L., Sinha, A., Harshuk, D., Cirigliano, A., Gurevich, S., Yu, Z., et al. (2019) The proteasome lid triggers COP9 signalosome activity during the transition of *Saccharomyces cerevisiae* cells into quiescence. *Biomolecules* **9**, 449
71. Torggler, R., Papinski, D., Brach, T., Bas, L., Schuschnig, M., Pfaffenwimmer, T., et al. (2016) Two independent pathways within selective autophagy converge to activate Atg1 kinase at the vacuole. *Mol. Cell.* **64**, 221–235
72. Goldstein, A. L., and McCusker, J. H. (1999) Three new dominant drug resistance cassettes for gene disruption in *Saccharomyces cerevisiae*. *Yeast* **15**, 1541–1553
73. Aranda-Díaz, A., Mace, K., Zuleta, I., Harrigan, P., and El-Samad, H. (2017) Robust synthetic circuits for two-dimensional control of gene expression in yeast. *ACS Synth. Biol.* **6**, 545–554
74. Gnügge, R., Liphardt, T., and Rudolf, F. (2016) A shuttle vector series for precise genetic engineering of *Saccharomyces cerevisiae*. *Yeast* **33**, 83–98
75. Shen, M. W. Y., Fang, F., Sandmeyer, S., and Da Silva, N. A. (2012) Development and characterization of a vector set with regulated promoters for systematic metabolic engineering in *Saccharomyces cerevisiae*. *Yeast* **29**, 495–503